University of Glasgow | School of Physics & Astronomy

Astronomy 345: Heliophysics & Stellar Atmospheres II

Session 2023-24

11 Lectures, starting January 2024

Lecturer: Prof. Eduard Kontar
Kelvin Building, room 615, extension x2499
Email: Eduard.Kontar (at) glasgow.ac.uk

Lecture notes and example problems - https://moodle.gla.ac.uk/course/view.php?id=40473

last update: July 17, 2024 at 01:05:25

Contents

1 Introduction to Solar Atmosphere 3
2 Density and opacity of the solar atmosphere 20
3 Radiation and thermal conduction 37
4 Static and dynamic equilibria of the solar corona 48
5 Wind solutions and solar wind 60
6 Observations and effects of the solar wind 70
7 Radiatively driven winds 82
8 Observed line profiles: P-Cygni profiles 94
9 Magnetic solar atmosphere 107
10 The effects of magnetic field 120
11 Plasma turbulence and coronal heating 133

1 Introduction to Solar Atmosphere

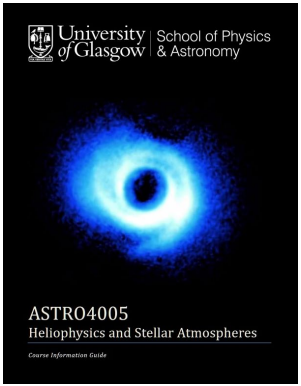
LECTURE OUTLINE

- Intended learning outcomes
- Recommended literature
- Solar Atmosphere Observations

1.1 Course aims

To introduce students to the physical processes responsible for

- Solar atmospheric structure
- Static and dynamic equilibria of the solar corona
- Radiatively driven winds
- Solar wind



Further details are also available in Course Handbook

1.2 Recommended literature and useful resources:

These lecture notes are following the material from:

An introduction to modern astrophysics by Carroll, Bradley & Ostlie, Dale, 2017, Second edition.UofG Library

Introduction to stellar winds by H. Lamers & J. Cassinelli; Cambridge University Press, 1999. UofG Library

High energy astrophysics, volume 1 & 2 by Malcolm S. Longair UofG Library

Online lectures:

Plasma Physics (solar wind section) by Richard Fitzpatrick

1.3 The Sun's atmosphere

The solar atmosphere is often divided in layers (see Figure 1.1) [1]

- **photosphere**
- **chromosphere**
- **transition region**
- **corona**

The solar surface is defined as the location in the photosphere where the solar gas is opaque at wavelength 500 nm.

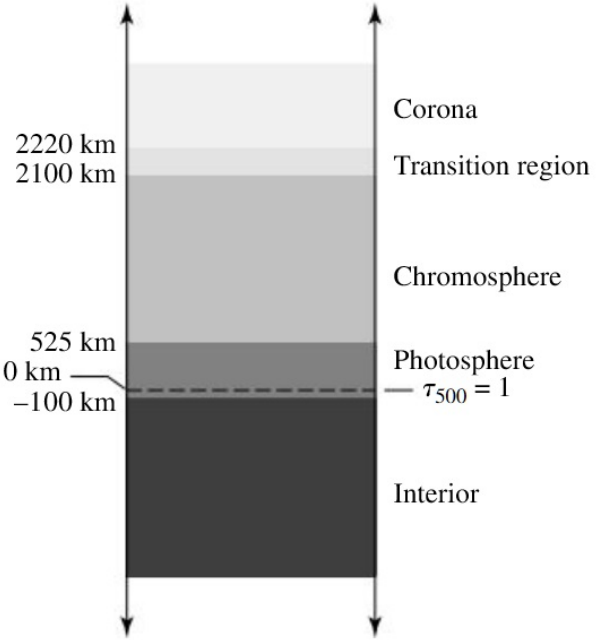


Figure 1.1: *The thickness of the components of the solar atmosphere from Fig 11.12 in Carroll, Ostlie 2017*

[1] Recall Astronomy 1 course on Solar System

1.4 Solar atmosphere density and temperature

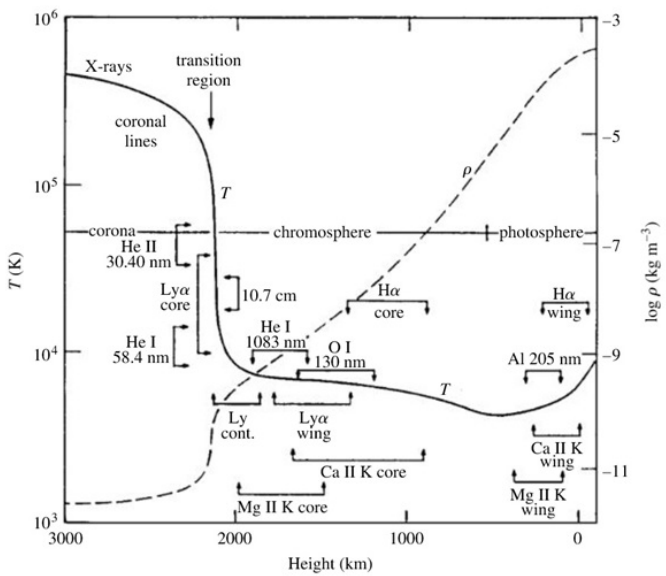


Figure 1.2: *Temperature structure (solid line) and density structure (dashed line) of the solar atmosphere. The altitudes observed at various wavelengths are indicated.*

Typical plasma temperatures:

Photosphere $\sim$ 5800 K.
Chromosphere from $\sim$ 4000 to $\sim$ 10^4 K.
Transition region from $\sim$ 10^4 to $\sim$ 10^6 K.
Corona has temperature $1 - 2$ MK.

Observations in **different wavelengths** are required to see different layers of the solar atmosphere. Plasma density $\rho = m_{\text{particle}} n$ [kg m^{-3}], where m_{particle} is the average particle mass and n is the number density [m^{-3}].

1.5 Multi-wavelength observations

Spot the differences in these 4 images of the Sun in figure 1.3.

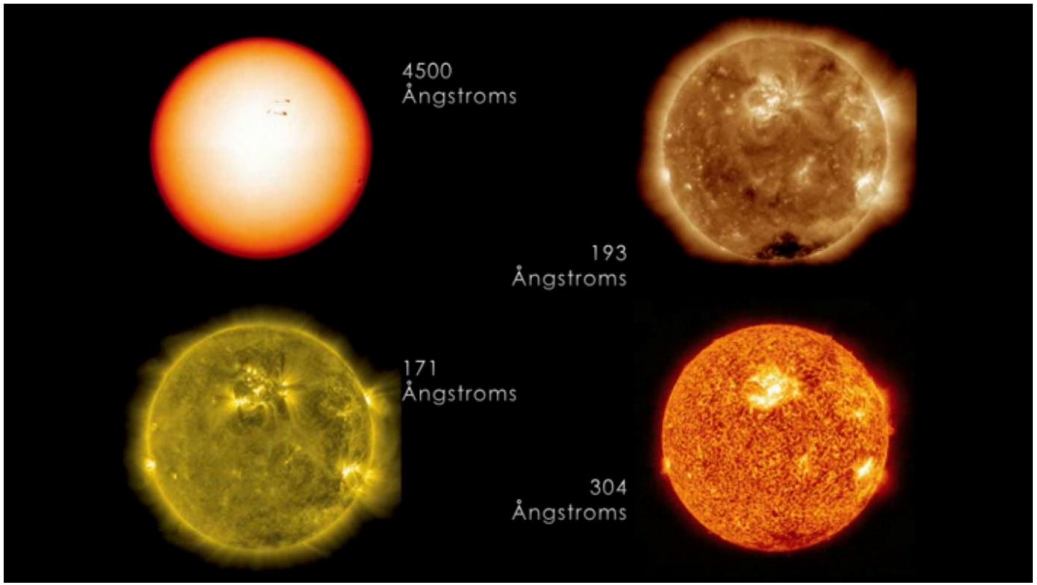


Figure 1.3: *Simultaneous views of the Sun from the AIA telescope on board SDO using four different filters. Can you guess which regions of the solar atmosphere are seen here? from http://aia.lmsal.com*

1.6 Photosphere features

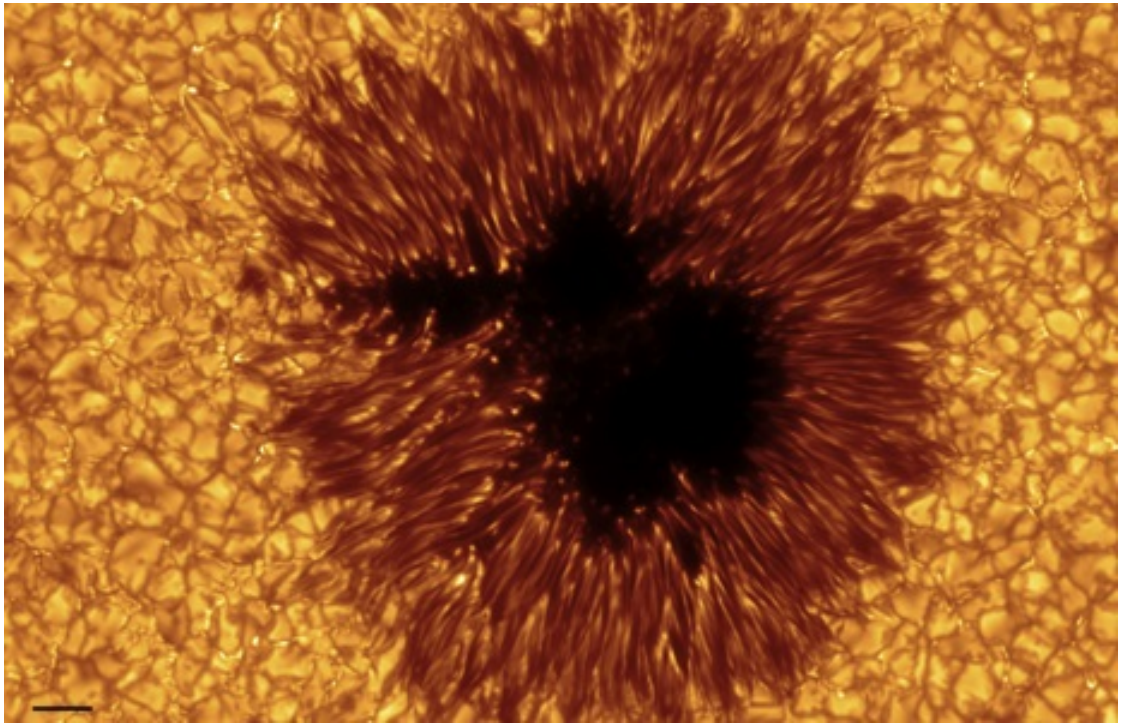


Figure 1.4: *Photospheric **granules** and cooler regions called **sunspot** (dark area is umbra surrounded by brighter region penumbra).*

1.7 Features of the chromosphere

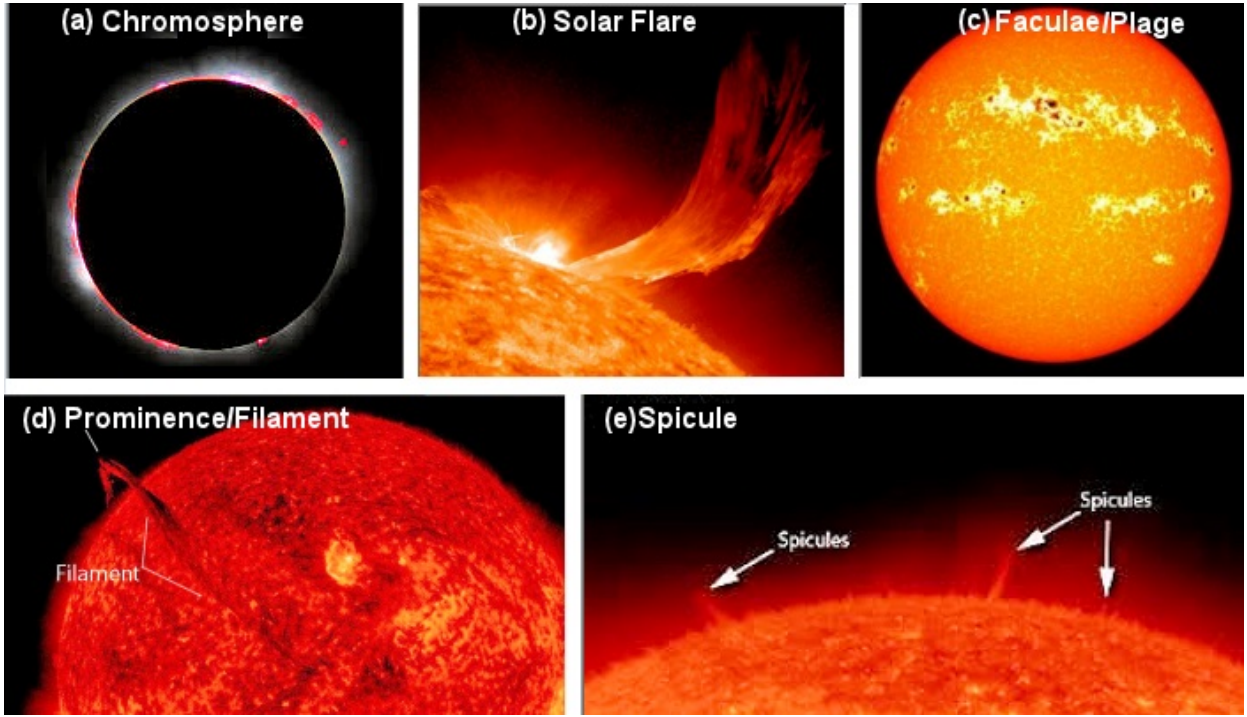


Figure 1.5: *Features of the chromosphere (mostly in Hα light): Plage (bright region typically around sunspots), prominence, spicules (transient vertical features), solar flares: image from universe-review.ca*

1.8 Corona features



Figure 1.6: *Total Solar Eclipse Corona in visible light. Note higher density features structured by magnetic field: coronal loops, streamers, active regions. image from NASA/APOD*

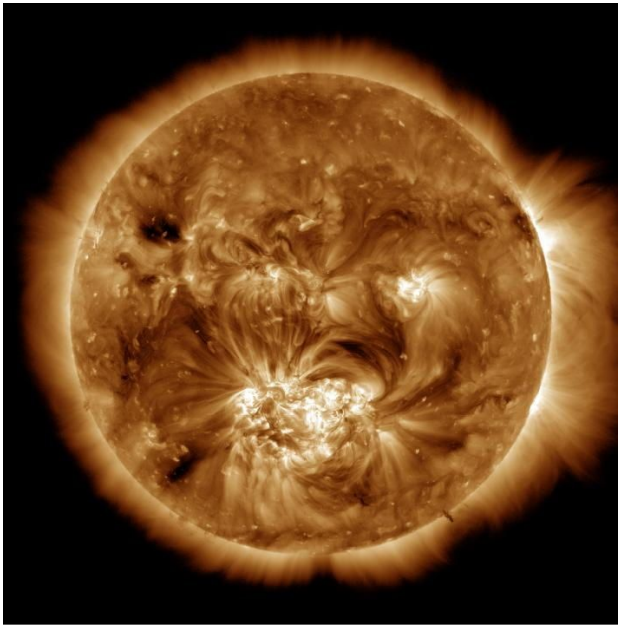


Figure 1.7: *1.5 MK solar corona plasma imaged by NASA SDO/AIA Note: coronal holes (dark regions of cooler plasma), active regions (brighter regions) and magnetic loops. Image from NASA/SDO*

1.9 Why does the solar disc have a sharp edge?

To start with, let us have a quick look at how the Sun looks like in visible light (Figure 1.8). We define the solar edge as the position where the **optical thickness** drops to $\tau \ll 1$. This happens (in the visible) at the photosphere.

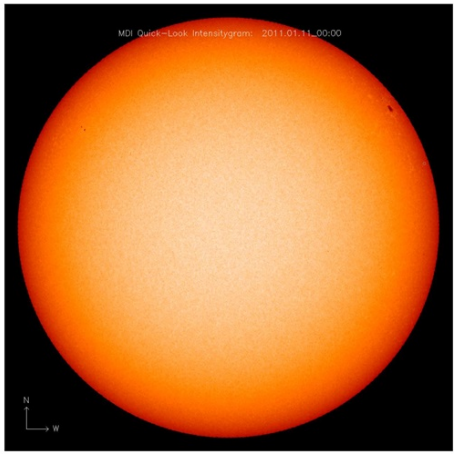


Figure 1.8: *An image of the Sun obtained in the visible range with the Michelson Doppler Imager (MDI) instrument on board the Solar and Heliospheric Observatory (SOHO) spacecraft. See http: soi.stanford.edu for more.*

The optical thickness[2] is a measure of transparency of the atmosphere and may be thought of as the number of **mean free paths** ℓ from the origin of a light ray to the surface (of that atmosphere), as measured along the ray's path. For an homogeneous plasma, the mean free path is

$$\ell = \frac{1}{n\sigma_T}, \tag{1.1}$$

[2] Recall HSA I lectures

where n is the electron number density m^{-3} and the Thomson scattering cross-section is

$$\sigma_T = \frac{8\pi}{3}\left(\frac{e^2}{4\pi\epsilon_0 m_\mathrm{e} c^2}\right)^2 \approx 6.65 \times 10^{-29}\ \mathrm{m}^2 \qquad (1.2)$$

Inside the Sun, the opacity is large due to Thomson scattering, when a photon is scattered off a free electron (no change in energy of the photon). Since the optical thickness of an atmospheric layer of geometrical thickness D is given by

$$\tau = \int_0^D \frac{\mathrm{d}z}{l} = \int_0^D n\sigma_T\,\mathrm{d}z, \qquad (1.3)$$

where dz is a path element, we need to investigate how the electron density n changes with height z in the outer layers of the Sun before being able to explain the sharp (visible) edge of the Sun.

In general the optical thickness varies with wavelength, and the above definition only refers to the case where the only relevant mechanism for photon interaction is Thomson scattering. It is therefore not applicable to all regions of the electromagnetic spectrum, e.g. when spectral lines are present.

The emission originating from photosphere is scattered away or absorbed along the line of sight and we see **limb darkening** because the higher optical thickness (larger path for photons along to the limb rather than to the center of the Sun).

The optically thin emission from the solar atmosphere is showing **limb brightening** (e.g. 193Å emission in Figure 1.3) as the thickness of emitting plasma along the line of sight is larger near the limb. Optically thin bremsstrahlung emission luminosity from volume V is $L \propto \int n_e n_{ion} dV$.

1.10 Isothermal atmosphere in hydrostatic equilibrium

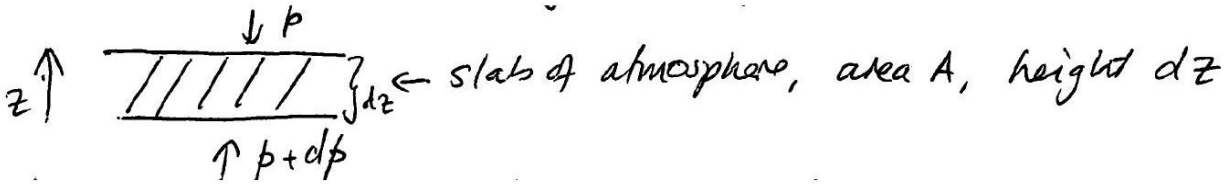


Figure 1.9: *Sketch of a slab of atmosphere of thickness* dz*, area* A*.*

Consider a slab of atmosphere (Fig. 1.9) of density ρ in a static (non-moving) equilibrium, so that the pressure excess, dp, balances the weight:

$$A\,\mathrm{d}p = -\rho A\,\mathrm{d}z g. \tag{1.4}$$

This yields

$$\frac{\mathrm{d}p}{\mathrm{d}z} = -\rho g \tag{1.5}$$

Now let us assume that the atmosphere is made of fully ionised hydrogen of temperature T, and that the gravitational acceleration does not vary

significantly with height. Since there are n electrons and n protons per unit volume, the equation of state is

$$p = 2nk_BT = \underbrace{nk_BT}_{\text{electrons}} + \underbrace{nk_BT}_{\text{protons}} \tag{1.6}$$

where we assume isothermal plasma $T_e = T_i$.

Thus

$$\frac{\mathrm{d}p}{\mathrm{d}z} = 2kT\frac{\mathrm{d}n}{\mathrm{d}z} = -nm_{\mathrm{p}}g$$

with m_{p} the mass of the proton. This has solution

$$n(z) = n_0 e^{-z/h}, \quad \text{where} \quad h = \frac{2kT}{m_{\mathrm{p}}g}. \tag{1.7}$$

where h is the scale height. and note that the electron density n drops exponentially with each multiple of h. Taking $T = 6000$ K for the Sun, we get $h_\odot \approx 360$ km, which is an overestimate.

At $T = 6000$ K, hydrogen is weakly ionised, and the gas pressure is $p = nk_B T$, so $h_\odot \approx 180$ km.

Going back to the total optical thickness, from Eq.1.3, one finds

$$\tau = \int_0^\infty n(z)\sigma_T \, \mathrm{d}z = \int_0^\infty n_0 e^{-z/h}\sigma_T \, \mathrm{d}z = \sigma_T n_0 h.$$

If we set $\tau = 1$, the electron number density at the surface is therefore $n_0 = \frac{1}{\sigma_T h} \simeq 10^{23}$ m^{-3}.

Comments:

• $\tau \propto n$, so τ drops exponentially with height (again with scale height $h_\odot \approx 180$ km $\ll R_\odot$). This is why we see a sharp edge to the photosphere: τ goes from $\gg 1$ to $\ll 1$ in about 10^{-3} of the solar radius.

• The mean free path of photons is $\frac{1}{n\sigma_T} = h_\odot = 180$ km, while the collisional mean free path of atoms is ≈ 1 mm. So we would expect photons to be able to leave the Sun, while atoms would still be confined.

• The solar atmosphere is not pure hydrogen, but has heavier elements, so the mean particle mass is $\simeq 1.27 m_p$, which would give agreement with models and observations (Figure 1.10.)

• The solar photosphere is weakly ionised, but the corona is fully ionised (Figure 1.10.)

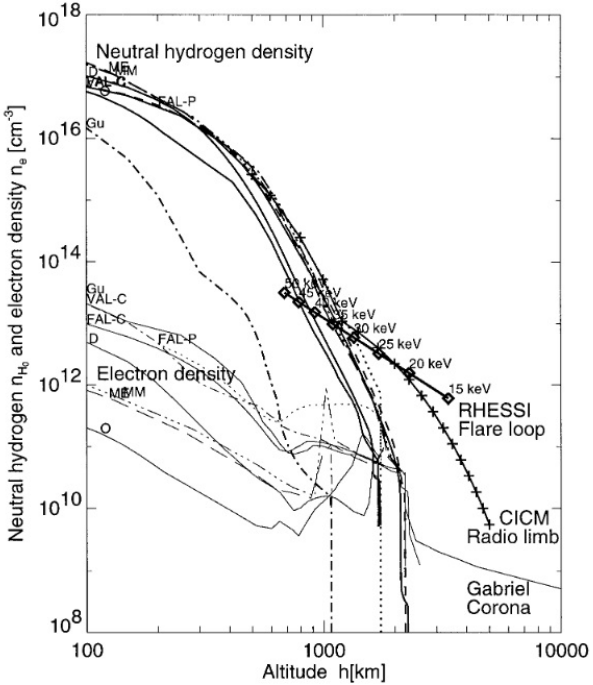


Figure 1.10: *A compilation of chromospheric and coronal density models from Aschwanden 2002 for more. Note exponential profile below* 10^3 *km.*

1.11 Element abundances

Element	Atomic Number	Log Relative Abundance
Hydrogen	1	12.00
Helium	2	10.93 ± 0.004
Oxygen	8	8.83 ± 0.06
Carbon	6	8.52 ± 0.06
Neon	10	8.08 ± 0.06
Nitrogen	7	7.92 ± 0.06
Magnesium	12	7.58 ± 0.05
Silicon	14	7.55 ± 0.05
Iron	26	7.50 ± 0.05
Sulfur	16	7.33 ± 0.11
Aluminum	13	6.47 ± 0.07
Argon	18	6.40 ± 0.06
Calcium	20	6.36 ± 0.02
Sodium	11	6.33 ± 0.03
Nickel	28	6.25 ± 0.04

Figure 1.11: *The relative abundance of elements is given by* $\log_{10}(N_{element}/N_H)+12$ *from Grevesse and Sauval, 1998*

The most abundant elements in the solar photosphere are given in Table 1.11. Considering Helium

$$\log_{10}(N_{\rm He}/N_{\rm H}) + 12 \simeq 10.93$$

so by number helium is $\sim 8.5\%$, so by mass Helium (2 protons and 2 neutrons) is $\sim 24\%$ and the mean mass per atom is $\mu \sim (1. + 0.24)m_p$ or more precisely $\simeq 1.27m_p$ (Figure 1.10.)

Minor ions in the solar atmosphere are useful for **plasma diagnostics**. Note e.g. 193 Å a spectral line emitted by iron atoms that have lost 11 electrons (also known as iron-12 or Fe XII) in Fig 1.7.

2 Density and opacity of the solar atmosphere

LECTURE OUTLINE

- Density and opacity
- Absorption and emission lines
- Solar chromosphere temperature
- Temperature increase and heating problem

2.1 Sun's surface

Recall from HSAI, that for a plane-parallel grey atmosphere (with $\tau \neq \tau(\lambda)$), the temperature at optical depth [1]τ is:

$$T = T_{eff}\left(\frac{1}{4}(3\tau + 2)\right)^{1/4}, \qquad (2.1)$$

with T_{eff} the effective temperature obtained from $L = 4\pi R^2 \sigma T_{eff}^4$. In such a grey atmosphere, when $T = T_{eff}$, we have $\tau = 2/3$: we mostly see material in the **photosphere** at $\tau = 2/3$ (Fig. 2.1).

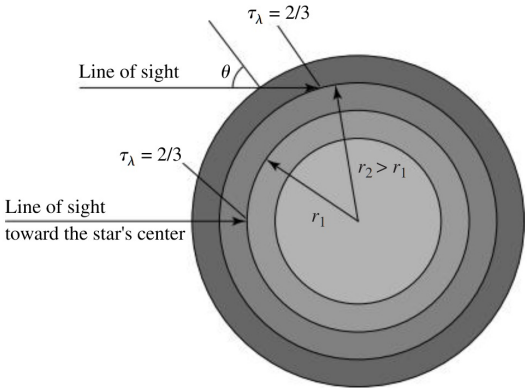


Figure 2.1: *Limb darkening. To reach a specified optical depth (e.g. $\tau = 2/3$), the line of sight terminates at greater distances.*

However, in general $\tau = \tau(\lambda)$, [3] usually decreasing as z increases. If the opacity is large at some λ, we see emission from (normally cooler) material

[3] The optical depth is the optical path-length along the line of sight, against the direction of photon propagation, from outside the object into it.

higher up in the atmosphere. Kirchoff's laws tell us that **absorption lines** will be observed (Fig. 2.2). This also explains why we observe limb darkening (recall Figure 1.8).

The solar spectrum also contains **emission lines** (recall Figure 1.3), so there must be material above the photosphere that is hotter than the photosphere.

Figure 2.3 shows a schematic temperature vs. height plot to illustrate this.

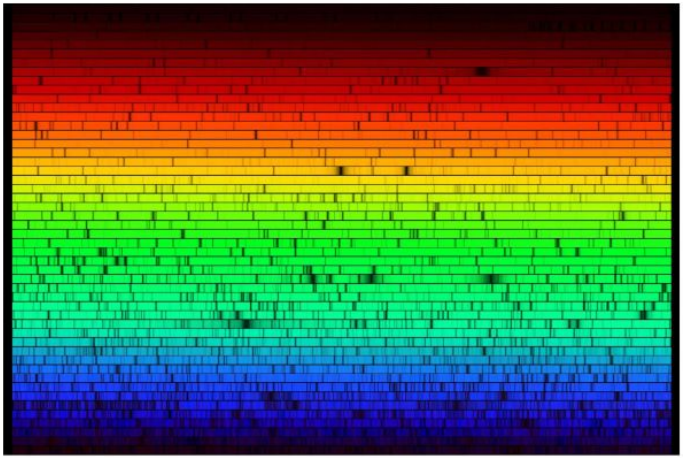


Figure 2.2: *A high-resolution version of the spectrum of our Sun from 400 to* 700 nm*. Absorption lines are seen as dark vertical features. Source: N.A.Sharp, NOAO/NSO/Kitt Peak FTS/AURA/NSF. solarsystem.nasa.gov*

2.2 Absorption and emission lines

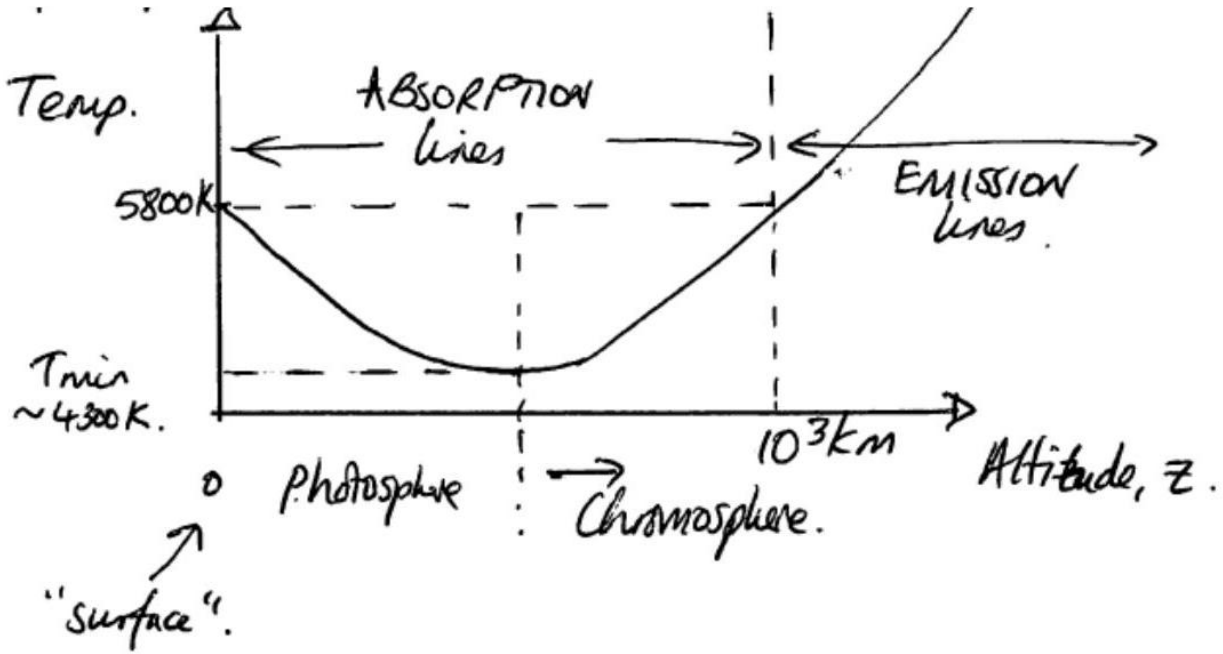


Figure 2.3: *Sketch of temperature change with height in the lower part of the solar atmosphere. Emission lines arise in the region where the temperature is larger than at the solar surface. The chromosphere (layer above the photosphere) starts above the temperature minimum.*

2.3 Observed solar flux spectrum

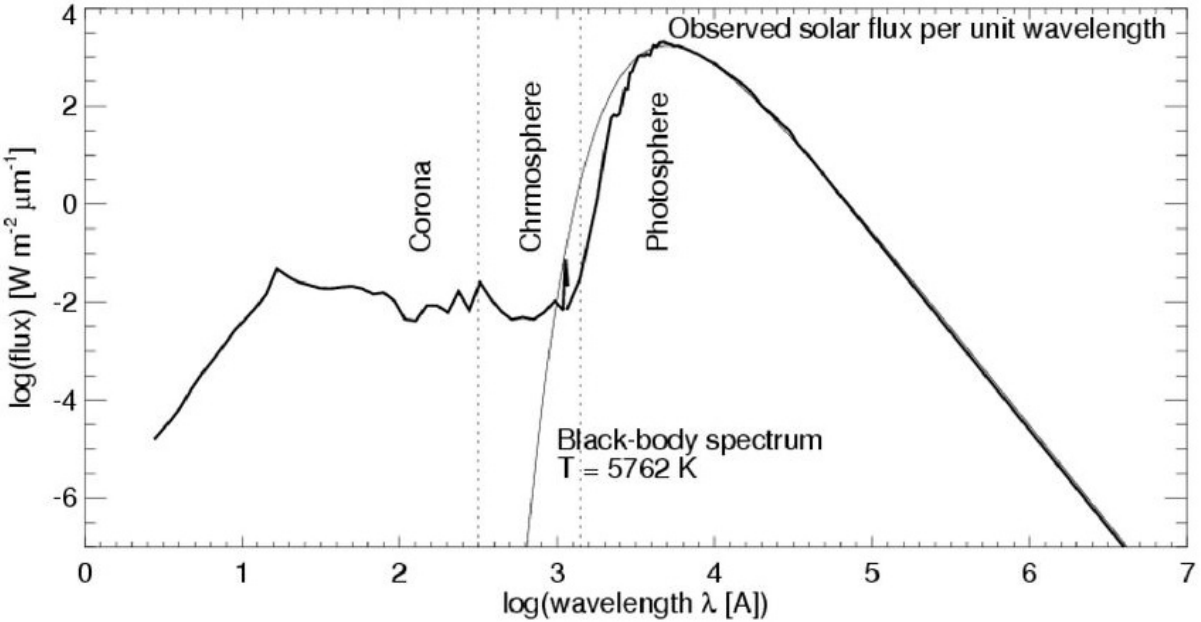


Figure 2.4: *Observed solar flux spectrum from Brian Dennis (NASA summer school)*

2.4 Sun's chromosphere

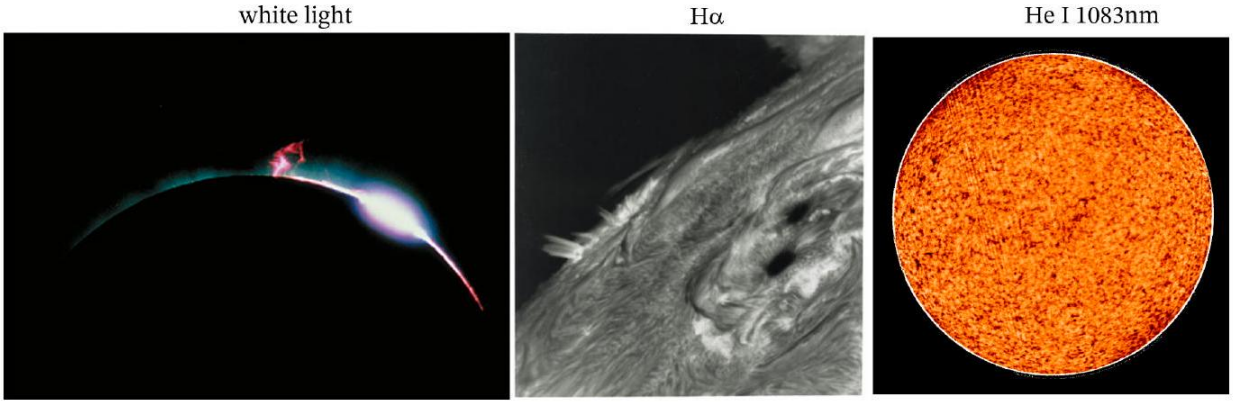


Figure 2.5: *Three views of the solar chromosphere.*

The **chromosphere** (Figure 2.5) is optically thin in continuum regions, but optically thick for bright lines such as Hα, or strong resonance lines (i.e. transitions to the ground state of the atom or ion) emitted by He I, He II, Ca II.[4]

[42] XI denotes the neutral (atomic) form of element X, while X II is once ionised, X III is twice ionised, etc.

Solar **chromosphere** is revealed by **pink/redish emission**[5] in eclipse images:

- pink because of $H\alpha$,
- emission because it is hotter than the photosphere
- eclipses mask the bright disc of the Sun, allowing the fainter outer layers (chromosphere and corona) to be seen.

But the chromosphere can also be observed directly by tuning a telescope to the wavelength of these strong emission lines (e.g. by using Hα filters). Such observations show that it has a "hairy" structure in places, due to the presence of spicules.

Observations show us also that the Sun is enveloped in a large, very hot $(\sim 10^6$ K$)$ region called the **corona**.[6] The chromosphere connects the photo-

[5] It was named after the Greek root chroma (meaning color).

[6] Corona (Latin for 'crown') is, in turn, derived from Ancient Greek.

sphere to the corona. Between the $\sim 10^4$ K chromosphere and the $\sim 10^6$ K corona is the **transition region** which is ~ 100 km thick.

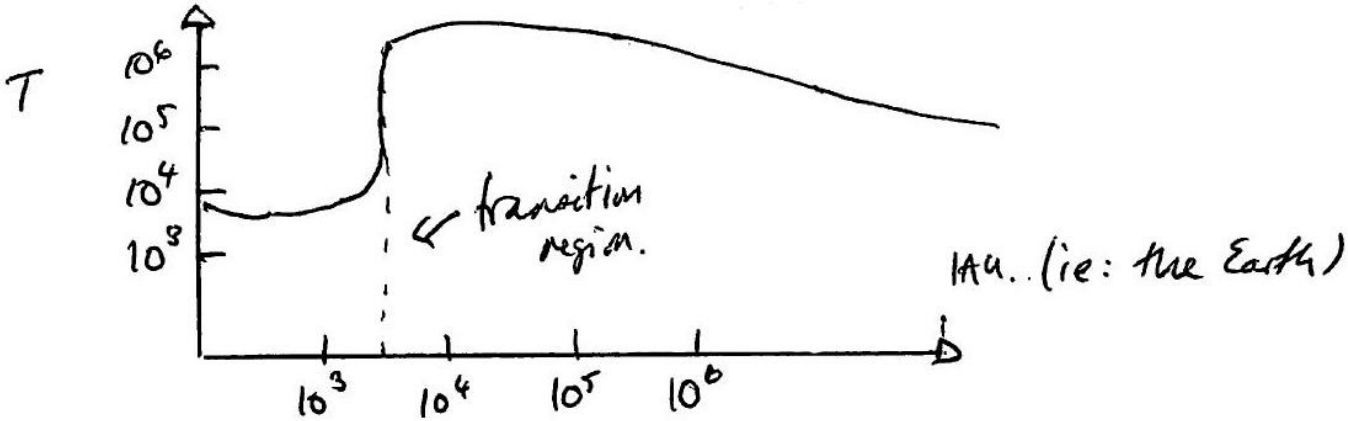


Figure 2.6: *Temperature of solar atmosphere vs height.*

Figure 2.6 shows a schematic temperature vs height plot emphasising how (geometrically) thin the transition region is compared to the chromosphere and the corona.

2.5 Solar corona

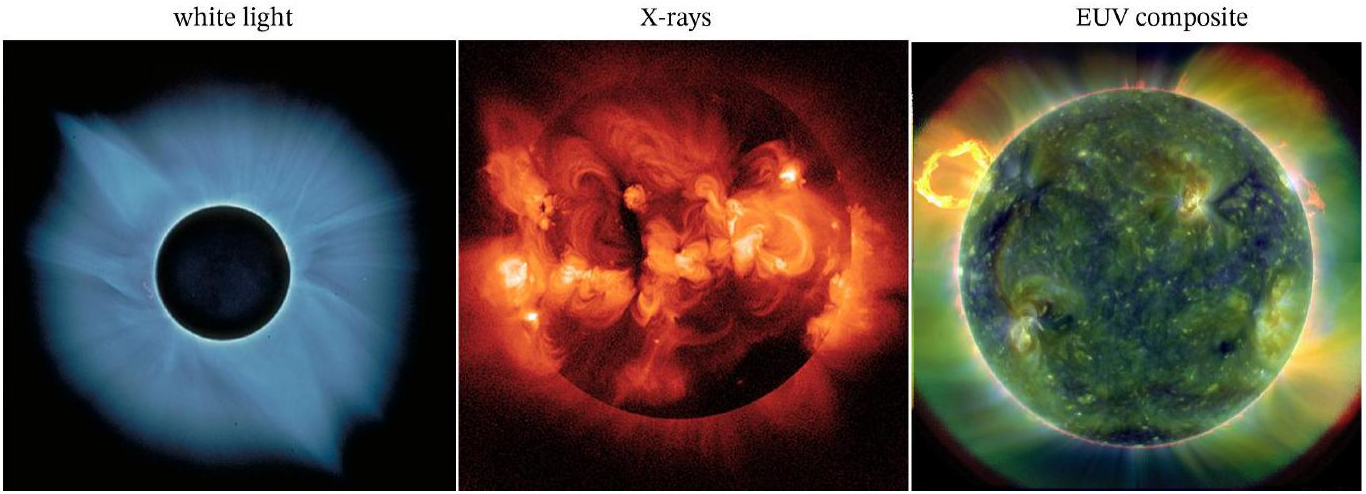


Figure 2.7: *Three views of the solar corona.*

The corona extends to several solar radii. It can be observed across the electromagnetic spectrum, but most notably in X-ray emission lines and continua, in UV/XUV emission lines, or by white-light scattering (Fig. 2.7).

2.6 Optically thin emission lines in the solar corona

The intensity of an emission line from volume ΔV can thus be written as:

$$I(\lambda) = \frac{1}{4\pi d^2} \int_{\Delta V} G_{\text{th}}(T, N_e) N_e N_H dV$$

where d is the distance to the source. The quantity $N_e N_H dV = d(\text{EM})$ defines the amount of plasma at different temperatures in the volume dV. The total EM of the plasma is given by integrating over the total emitting volume V:

$$EM = \int_V N_e N_H dV \quad [m^{-3}]$$

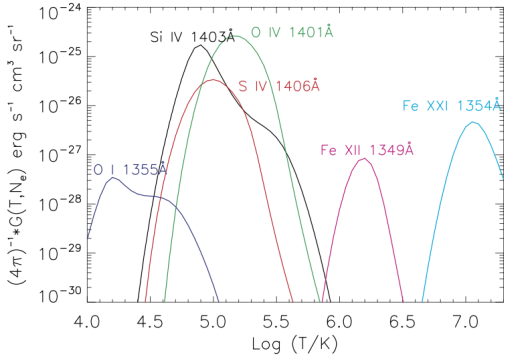


Figure 2.8: *Contribution functions (in a log scale) for a set of spectral lines.* $1\ erg = 10^{-7}\ J$.

2.7 Coronal heating problem

One would expect that without any addition energy input the solar atmosphere is nearly isothermal $\sim 6 \times 10^3$ K or decreasing due to energy losses, but we observe $\sim 10^6$ K, which is 100-150 times hotter.

Why are the chromosphere and the corona hotter than the photosphere? How is the chromosphere heated (it cannot be via conduction from the cooler photosphere because thermodynamics demands that heat flows from hot to cold)? **These are some of the most important questions in astrophysics.**

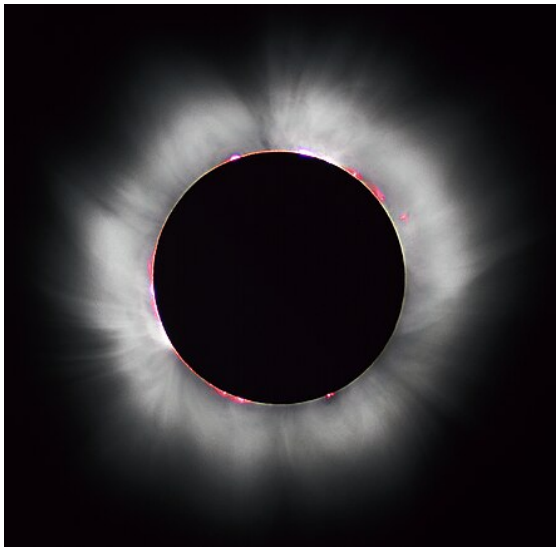


Figure 2.9: *During a total solar eclipse, the Sun's corona and prominences are visible to the naked eye.*

2.8 Explaining the increase in temperature with height

The increase in temperature with height cannot be explained by **thermal conduction**: heat flows from hotter to cooler regions. Indeed, heat flows are observed from the corona towards the photosphere. We therefore need a mechanical (not thermal) transport mechanism to damp energy in the corona. There are two main candidates.

2.9 Acoustic (sound) waves

These are **sound waves** produced by the motion of the solar surface, and they propagate upwards. As the number density of particles decreases with height, the wave amplitude must increase in order to preserve the energy flux. Waves then become **shock waves** and dissipate as thermal energy in the corona.

Indeed, sound waves are prorogating fluctuations of density (compressions), so the sound speed is probational to square root of pressure (restoring force) and inversely proportional to mass density (inertia)

$$c = \sqrt{\frac{\gamma P}{\rho}} \tag{2.2}$$

where γ is adiabatic index. For ideal hydrogen (e.g. $\rho = nm_{\mathrm{p}}$) gas $p = nk_B T$, we have $c = \sqrt{\gamma k_B T / m_p}$, where $\gamma = 5/3$.

If the energy flux of sound waves with amplitude δv is conserved, i.e.

$$\frac{\rho \delta v^2}{2} c = \text{const}$$

then since density ρ decreases with height, the amplitude of sound waves grows with height, while the sound speed c is virtually a constant. So the wave could become $\delta v > c$ creating a **shock wave**. As the shock moves through the gas, it can efficiently heat the gas.

Thus, photospheric motions could generate sound waves and heat chromosphere.[7] However, sound wave heating only work low down, i.e. mostly in the chromosphere: acoustic waves either break too early, or are reflected back towards the chromosphere, to be able to explain the high coronal temperatures.

[7] This is actively debated topic Kalkofen, 2007

2.10 Magnetic waves

Several mechanisms are possible. Essentially, the magnetic field acts like stretched elastic bands, allowing **Alfvén waves** (low-frequency plasma oscillations) to propagate into the corona[8]. These then damp energy. Spicules (Fig. 2.10), and other structures observed in the Sun's corona, support this idea.

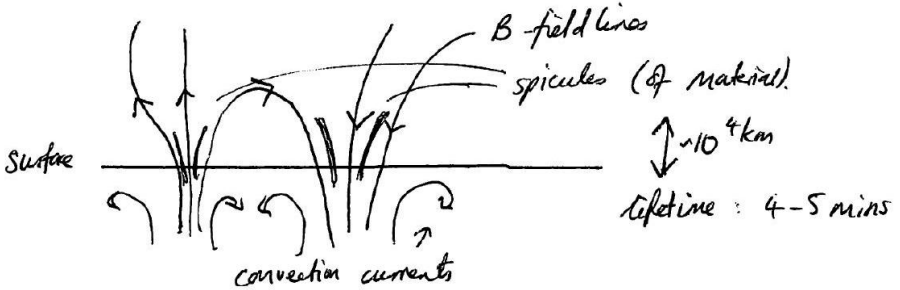


Figure 2.10: *Sketch of spicules within the (simplified) solar magnetic environment.*

As magnetic field creates pressure $B^2/(2\mu_0)$, where μ_0 is the permeability of empty space. By analogy with sound waves, **Alfven speed** should be

[8] Introduced by H. Alfven Alfven, 1942

proportional to the square root of magnetic pressure (restoring force), so we write

$$v_{\mathrm{A}} = \sqrt{\frac{B^2}{\mu_0 \rho}} = \frac{B}{\sqrt{\mu_0 \rho}}, \tag{2.3}$$

where v_{A} is Alfven speed.

Unlike sound waves, Alfven waves are (incompressible, i.e. no density fluctuations) magnetic fluctuations, i.e. magnetic tension balanced by plasma inertia.

The Alfven waves prorogate along magnetic field lines, they may transport energy outward. The dissipation of waves can contribute to the temperature structure of the solar corona e.g. Browning, 1991.

Alfven waves are observed in solar wind, see e.g. Belcher & Davis, 1971 and are believed (details are debated) to dissipate their energy in the solar wind via **turbulent cascade** to smaller scales.

3 Radiation and thermal conduction

LECTURE OUTLINE

- Radiation and radiative losses
- Thermal conduction

3.1 Radiative losses

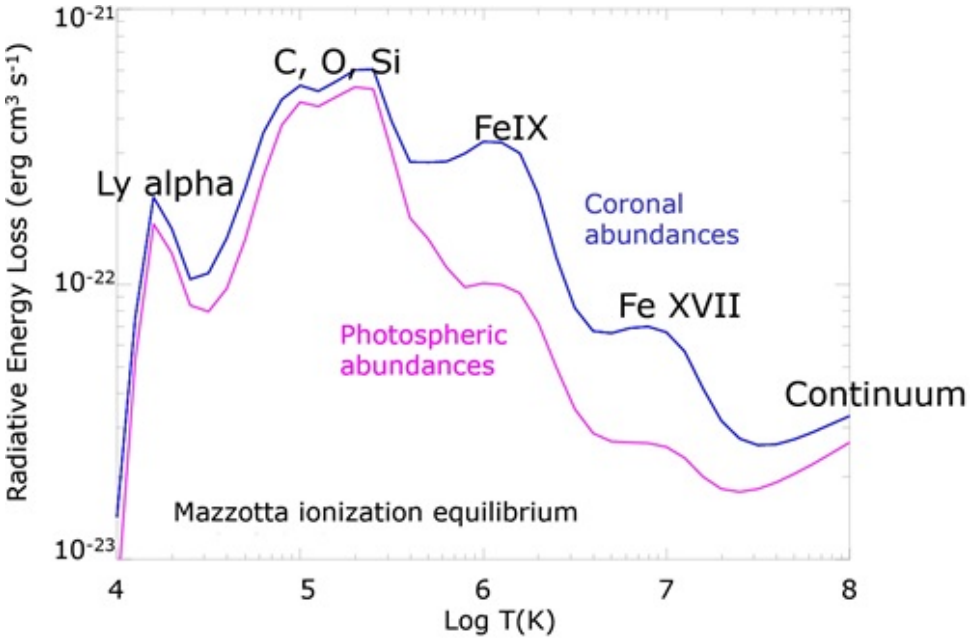


Figure 3.1: *Radiative energy loss as a function of temperature from Brian Dennis (NASA summer school). note that 1 erg* $=10^{-7}$ *J and the radiative energy loss depends on element abundances.*

Solar plasma (e.g. Fig 2.4) radiates both continuum and lines. In addition, the heat is transported from hotter to cooler regions of plasma via **thermal conduction** (recall the second law of thermodynamics). The heating mechanism should compensate for these energy losses.

3.2 Radiative instability

We want to explain the sudden jump in temperature seen in the transition region. We will consider a simple model that neglects thermal conduction and any mass motion in or out of the transition region. In a stable state, the plasma (fully ionised and at a temperature T) receives as much power in (via heating) as it lets power out (via cooling).

We assume that the plasma, with electron number density n, is heated at a constant rate per particle C :

$$\text{power in} \quad = Cn \quad [\text{ W m}^{-3}]$$

We also assume that the plasma is optically thin, and that the cooling is dominated by photon emission following collisional excitation between particles. The collisional excitation rate must be proportional to n^2, since two particles

are involved, and therefore:

$$\text{power out} \quad = f(T)n^2 \quad [\text{ W m}^{-3}].$$

The **radiative loss function** $f(T)$ depends on the collisional excitation rates, which depend on local temperature and intrinsic properties of the atoms and ions constituting the plasma.

Conservation of energy yields:

$$\frac{\mathrm{d}}{\mathrm{d}t}\left(\frac{3}{2}2nkT\right) = \underbrace{Cn}_{\text{heating}} - \underbrace{n^2 f(T)}_{\text{radiation}} \tag{3.1}$$

and therefore, since the number density n is constant (from our assumption of no mass flow):

$$\frac{\mathrm{d}T}{\mathrm{d}t} = \frac{C}{3k} - \frac{n}{3k}f(T). \tag{3.2}$$

Let us consider an **equilibrium situation** with $\frac{\mathrm{d}T}{\mathrm{d}t} = 0$ at a temperature T_0, and then perturb T such that $T = T_0 + \Delta T$. From Equation 3.2:

$$\frac{\mathrm{d}T_0}{\mathrm{d}t} + \frac{\mathrm{d}\Delta T}{\mathrm{d}t} = \frac{C}{3k} - \frac{n}{3k} f\left(T_0 + \Delta T\right).$$

By definition, $\frac{\mathrm{d}T_0}{\mathrm{d}t} = 0$. As we are only considering a small temperature perturbation, we can use a Taylor expansion for $f\left(T_0 + \Delta T\right)$.

$$\frac{\mathrm{d}\Delta T}{\mathrm{d}t} = \frac{C}{3k} - \frac{n}{3k} f\left(T_0\right) - \frac{n}{3k} \Delta T \left.\frac{\mathrm{d}f}{\mathrm{d}T}\right|_{T=T_0} + \cdots.$$

The first two terms on the RHS are $\frac{\mathrm{d}T_0}{\mathrm{d}t} = 0$. Thus

$$\frac{\mathrm{d}\Delta T}{\mathrm{d}t} = -\frac{n}{3k} f'\left(T_0\right) \Delta T$$

This differential equation has a solution:

$$\Delta T = \Delta T(0) \exp\left[-\frac{n f'\left(T_0\right)}{3k} t\right].$$

The stability of the system depends on the sign of f' : if $f' > 0$ it is **stable**, if $f' < 0$ it is **unstable**, i.e. this simple system is stable as long as the plasma radiates more when hotter, i.e. so long as $\frac{\mathrm{d}f(T)}{\mathrm{d}T} > 0$.

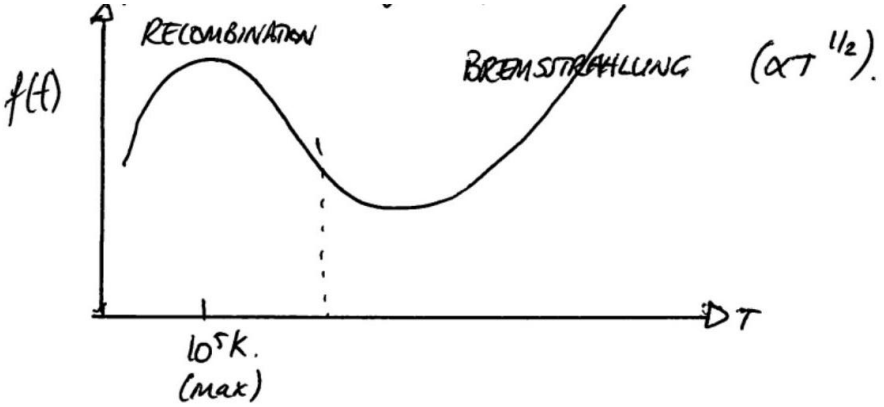


Figure 3.2: *Sketch of the temperature dependence of the radiative loss function in the solar atmosphere.*

The exact form of $f(T)$ depends on the relevant atomic processes, particularly on recombination rates. Its general form is illustrated in Fig. 3.2. In the recombination region, we look at the slope of $f(T)$: it is in equilibrium only when the slope is positive. Our model assumptions break down when the slope is negative.

What happens at the local maximum around $T_1 \sim 10^5$ K ? From Eq. 3.2, an equilibrium situation at temperature T_0 is such that

$$f(T_0) = \frac{C}{n} .$$

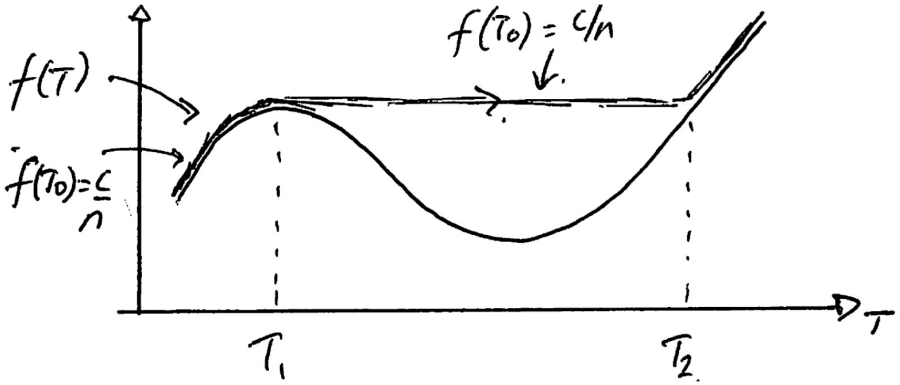


Figure 3.3: *Jump in equilibrium temperature.*

But as we look higher in the atmosphere, the density decreases, and $f(T_0)$ increases. The equilibrium temperature T_0 rises smoothly until T_1. Then a step transition occurs, and the equilibrium temperature jumps to the next accessible equilibrium temperature T_2 (Fig.3.3).

3.3 Thermal conduction

This steep jump in temperature defines the **transition region**, where another mechanism for energy loss takes over from radiation (therefore rendering our simple model inapplicable): thermal conduction of energy backwards towards the lower chromosphere. In general, the heat flux H (in Wm^{-2}) is proportional to the temperature gradient:

$$H = -\kappa \frac{\mathrm{d}T}{\mathrm{d}r}.$$

κ is the thermal conductivity. A simple model for it can be devised where we treat the plasma as a classical gas and we borrow a result from kinetic theory, yielding:

$$\kappa = \frac{1}{3}\rho \ell \bar{v} C_p. \tag{3.3}$$

ρ is the mass density ($\propto n$), $\bar{v}$ is the mean particle speed $\left(\propto T^{1/2}\right)$, and C_p is the heat capacity at constant pressure.

3.4 Heat conduction in collisional plasma

As before, the mean free path $\ell \propto \frac{1}{\sigma n}$, where σ is the relevant cross-section for the interaction under consideration. This time we are dealing with electron-proton collisions (**electrons being the mobile agents transporting energy**). So far we've established, looking carefully at Eq.3.3, that $\kappa \propto \frac{T^{1/2}}{\sigma}$, and is independent of the particle density n. We now want to know how the collision cross-section σ varies with temperature. In the broad sense, e-p collisions refer to interactions between electrons and protons: electrons are deflected when they come within a radius r of the proton (and then loose energy). For Coulomb interactions:

$$\frac{1}{2}mv^2 = \frac{e^2}{4\pi\epsilon_0 r}$$

From classical theory, $\frac{1}{2}mv^2 = \frac{3}{2}kT$, and thus $r \propto T^{-1}$, and collisional cross-

section $\sigma \approx \pi r^2 \propto T^{-2}$. This allows us to conclude that

$$\kappa = \kappa_0 T^{5/2} \text{(Spitzer thermal conductivity)}.$$

where $\kappa_0 \simeq 10^{-11}$ [$\mathrm{Wm^{-1}K^{-7/2}}$].

The heat flux is therefore

$$H = -\kappa_0 T^{5/2} \frac{\mathrm{d}T}{\mathrm{d}r}. \qquad (3.4)$$

This heat flux (in $\mathrm{Wm^{-2}}$) is conducted out of the transition region, and is balanced by a flux of power into the transition region - the exact nature of which is still under investigation. But this simple model explains fairly well the observed (small) thickness of the transition region.

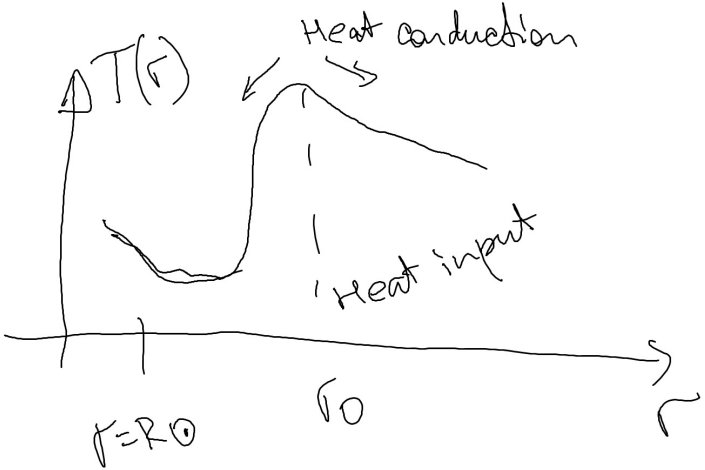


Figure 3.4: *Sketch of the temperature variation with height in the Sun's outer atmosphere, highlighting that heat conduction takes place from the base of the corona outwards and inward.*

3.5 Downward heat conduction in the corona

X-ray observations (Fig.3.5) indicate a steady radial increase of temperature in the corona out to $0.7-0.9R_\odot$ above the limb. The solid line shows the model with constant downward power $4\pi r_0^2 F_0$ by thermal conduction

$$-r_0^2 F_0 = -r^2 \kappa_0 T^{5/2} \frac{\mathrm{d}T}{\mathrm{d}r} \qquad (3.5)$$

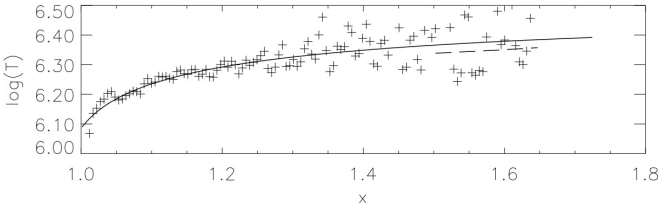


Figure 3.5: *Temperature values obtained from X-ray observations versus $x = r/R_\odot$. Solid line shows the thermal conduction model from Wheatland et al, 1997*

Integrating (3.5) with boundary condition $T(r = R_\odot) = T_0$

$$T(r) = \left[T_0^{7/2} + \frac{7R_\odot F_0}{2\kappa_0} \left(1 - \frac{R_\odot}{r} \right) \right]^{2/7},$$

where T_0 and F_0 are the temperature and the inward heat flux at the base of the corona, $r = R_\odot$, and κ_0 is the coefficient of thermal conductivity.

4 Static and dynamic equilibria of the solar corona

LECTURE OUTLINE

- equilibria of the solar corona
- temperature and density of the solar corona
- stellar wind theories

4.1 Outer layers of solar atmosphere

What happens past the transition region, higher up in the solar atmosphere? Observations show that in the outer atmospheric layers of the solar atmosphere:

1. the density n drops (which means bremsstrahlung also drops as it is $\propto n^2$),
2. the temperature is approximately constant.

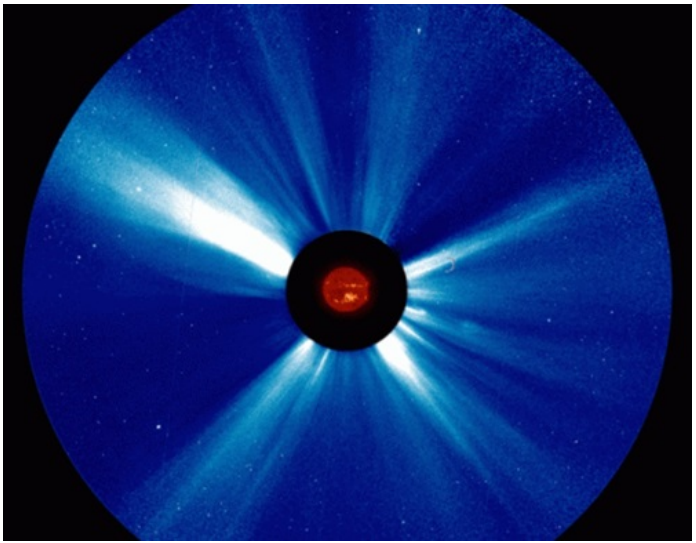


Figure 4.1: *Solar corona imaged by a coronograph from SOHO/ESA*

Can we have a static equilibrium given these observations (see e.g. Fig.4.1)?

4.2 Isothermal static corona

In this first attempt, we equate forces on a small section of atmosphere (see Fig. 4.2) which is made of fully ionised hydrogen:

$$A\,\mathrm{d}p = -\frac{GM\rho A\,\mathrm{d}r}{r^2}$$

$$\frac{\mathrm{d}p}{\mathrm{d}r} = -\frac{GM\rho}{r^2}$$

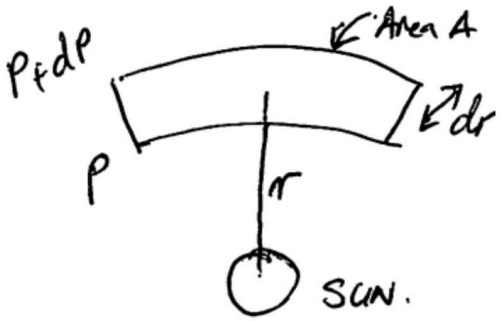


Figure 4.2: *Sketch of a section of the Sun's outer atmosphere.*

combining and using ideal gas-pressure $p = 2nkT$

$$\frac{\mathrm{d}}{\mathrm{d}r}(2nkT) = -\frac{GMnm_p}{r^2} \tag{4.1}$$

With only n varying with r, integrate this to obtain

$$n(r) = n_0 \exp\left(-a\left(1 - \frac{r_0}{r}\right)\right),$$

where a is a constant, and $n_0 = n(r_0)$.

The problem with this solution is that $n \to n_0 e^{-a}$ as $r \to \infty$, which means that there must be a finite number density (and finite pressure) at infinity. This is not physical and at odds with observations. This static isothermal model cannot work at $r \gg R_\odot$.

4.3 Non-isothermal static atmosphere

What would be an acceptable $T(r)$ profile for a hydrostatic atmosphere? We go back to Eq.4.1 but now differentiate both n and T with respect to r.

$$2k\left(T\frac{\mathrm{d}n}{\mathrm{d}r}+n\frac{\mathrm{d}T}{\mathrm{d}r}\right)+\frac{GMnm_p}{r^2}=0$$

$$\frac{1}{n}\frac{\mathrm{d}n}{\mathrm{d}r}+\frac{1}{T}\frac{\mathrm{d}T}{\mathrm{d}r}+\frac{GMm_p}{2kTr^2}=0$$

$$\ln\left[\frac{n(r)}{n_0}\right]+\ln\left[\frac{T(r)}{T_0}\right]=-\frac{GMm_p}{2k}\int_{r_0}^{r}\frac{\mathrm{d}r}{T(r)r^2}$$

$$\text{i.e. } n(r)T(r)=n_0T_0\exp\left[-\frac{GMm_p}{2k}\int_{r_0}^{r}\frac{\mathrm{d}r}{T(r)r^2}\right]$$

A static atmosphere requires $n(r)\to 0$ and $T(r)\to 0$ as $r\to\infty$. Hence we must have $\int_{r_0}^{r}\frac{\mathrm{d}r}{T(r)r^2}\to\infty$ as $r\to\infty$. This implies

$$T(r)\propto r^{-\alpha}\text{with }\alpha>1$$

4.4 Non-isothermal corona with thermal conduction

This idea is known as the **Chapman model** and suggests that the outer corona is heated by thermal conduction from the inner corona (Fig. 4.3). As usual, we start by considering the balance between the input power P_0 and the heat energy conducted through a spherical shell at radius r per second, both taken as constant (borrowing heat flux result from Eq. 3.4):

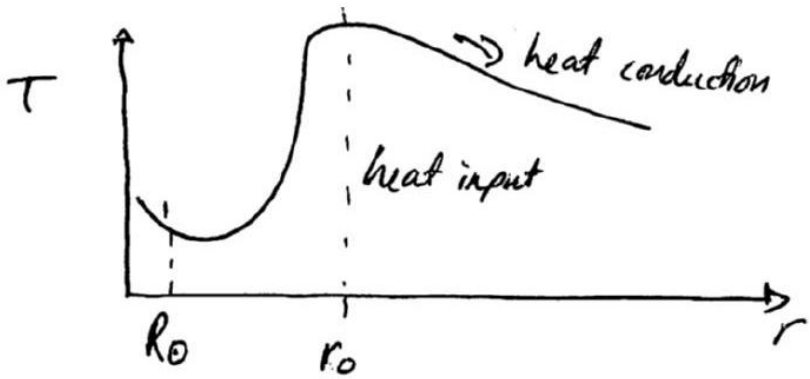


Figure 4.3: *Sketch of the temperature variation with height in the Sun's outer atmosphere, highlighting that heat conduction takes place from the base of the corona outwards.*

$$P_0 = -4\pi r^2 \kappa_0 T^{5/2} \frac{\mathrm{d}T}{\mathrm{d}r}$$

rearranging for T

$$T^{5/2}\,\mathrm{d}T = -\frac{P_0}{4\pi\kappa_0}\frac{\mathrm{d}r}{r^2}$$

and integration gives

$$\frac{2}{7}T^{7/2} = \frac{P_0}{4\pi\kappa_0}\frac{1}{r} + \text{constant.}$$

Our boundary conditions require $T \to 0$ as $r \to \infty$, and so the constant must be zero. This leaves

$$T(r) \propto r^{-2/7}$$

i.e. $\alpha = \frac{2}{7} < 1$. Therefore, this model cannot work either.

4.5 Pressure from the interstellar medium

It follows from the previous discussion that there does not seem to be static equilibrium possible for our isolated Sun's corona. Could the pressure from the interstellar medium (ISM) push back the outer corona to allow a finite, non-zero pressure at $r \to \infty$?

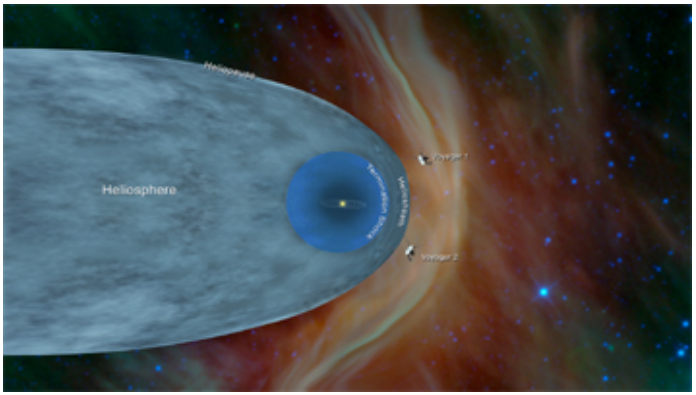


Figure 4.4: *This illustration shows the position of NASA's Voyager 1 and Voyager 2 probes, outside of the heliosphere from NASA JPL*

Sadly the answer is again no. The pressure from the Chapman model for instance is already 10^8 that of the pressure from the ISM at large distances, so the pressure from the ISM is not able to contain the solar corona.

4.6 Wind theories

The logical conclusion reached by E. Parker in 1958 is that the corona cannot be in hydrostatic equilibrium: we explicitly identify the coronal expansion flow as the solar wind.[9] A year later the solar wind speed was measured for the first time at 1AU at $\sim$ 300 km s^{-1}. In 2018, the Parker Solar Probe was launched by NASA to take more precise measurements closer to the Sun (Fig. 4.5).

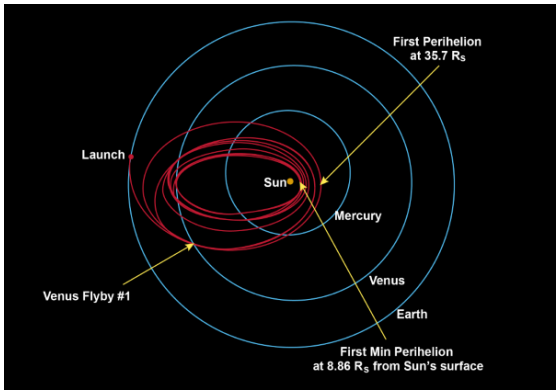


Figure 4.5: *NASA's Parker Solar Probe designed and is being built point out the instruments that will collect data as the mission travels directly through the Sun's atmosphere. Credits: NASA/JHUAPL*

We thus start with the simplest possible

[9] Of course we knew already then about the existence of the solar wind from comets' ion tails which are shaped by the local properties of the solar wind, as opposed to the dust tails which are shaped by radiation pressure.

model, i.e. an isothermal model, now including a steady, spherically symmetric mass flux. We can use the equation for mass continuity to write that

$$4\pi r^2 m_p n(r) v(r) = \dot{M} = \text{constant.} \tag{4.2}$$

where $\dot{M}$ is the rate of change of mass, i.e. the mass loss. $v(r)$ is the flow speed at distance r.

Now take Newton's Second Law $F = ma = m\frac{dv}{dt} = m\frac{dv}{dr}\frac{dr}{dt}$ for a small element of solar corona of volume Adr and mass $n(r)Adr$:

$$-A\,\mathrm{d}p - \frac{GMnm_pA\,\mathrm{d}r}{r^2} = A\,\mathrm{d}rnm_pv\frac{\mathrm{d}v}{\mathrm{d}r}$$

$$-\frac{\mathrm{d}p}{\mathrm{d}r} - \frac{GMm_pn}{r^2} = m_pnv\frac{\mathrm{d}v}{\mathrm{d}r}$$

This is saying that mass acceleration (RHS) is balanced by forces resulting from pressure gradient and gravitational attraction (LHS).

Using the equation of state for a fully ionised hydrogen plasma, we obtain

$$v\frac{\mathrm{d}v}{\mathrm{d}r} = -\frac{2kT}{m_p n}\frac{\mathrm{d}n}{\mathrm{d}r} - \frac{GM}{r^2}$$

$$v\frac{\mathrm{d}v}{\mathrm{d}r} = -\frac{2kT}{m_p}\frac{\mathrm{d}\ln n}{\mathrm{d}r} - \frac{GM}{r^2} \tag{4.3}$$

We need an expression for $\ln n$, which can be obtained from mass continuity Eq. 4.2 by taking ln:

$$\ln n = -2\ln r - \ln v + \text{constant}.$$

We insert this into Eq. 4.3 to obtain

$$\frac{1}{v}\frac{\mathrm{d}v}{\mathrm{d}r}\left(v^2 - \frac{2kT}{m_p}\right) = \frac{4kT}{m_p r} - \frac{GM}{r^2} \tag{4.4}$$

This can be rewritten as follows, after defining the sound speed as $c = \sqrt{P/\rho} = \sqrt{2kT/m_p}$:

$$\frac{1}{v}\frac{\mathrm{d}v}{\mathrm{d}r} = \frac{\frac{2c^2}{r}\left(1 - \frac{r_c}{r}\right)}{v^2 - c^2} \qquad (4.5)$$

We have introduced the critical radius $r_c = \frac{GM}{2c^2}$ at which the wind speed is equal to the sound speed. Note that when $r = r_c, \frac{\mathrm{d}v}{\mathrm{d}r} = 0$ unless $v = c$ (see Fig. 4.6).

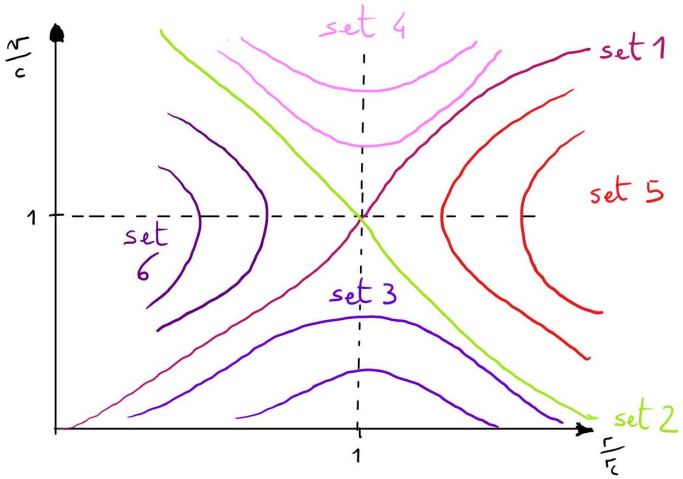


Figure 4.6: *The six sets of velocity profiles of isothermal solar winds.*

Solutions to Eq. 4.5 are known as the velocity profiles of isothermal solar winds:

$$\frac{v^2}{c^2} - 2\ln\frac{v}{c} = 4\ln\frac{r}{r_c} + 4\frac{r_c}{r} + \text{constant}\,. \qquad (4.6)$$

5 Wind solutions and solar wind

LECTURE OUTLINE

- different wind solution
- critical radius and speed
- solar wind solution

5.1 Different wind solutions

Depending on the value of the constant, there are six sets of solutions (Figs. 4.6 and 5.1 for various (constant) temperatures):

Types 5 and 6 are not continuous in r : we ignore these non-physical solutions.

Types 2 and 4 start supersonic $(v > c)$: we ignore these solutions as we don't observe a supersonic wind in the lower solar corona.

Type 3 starts and ends subsonic $(v < c)$: we ignore this for the moment as this does not match our observations, but we will come back to the concept of stellar breeze later.

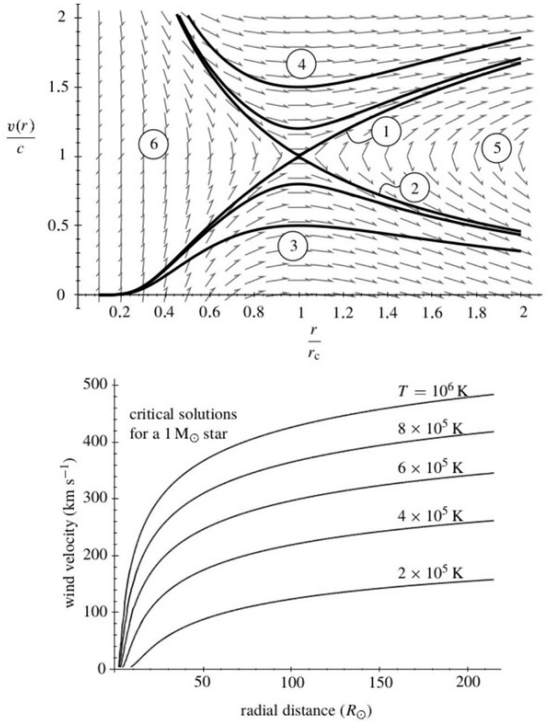


Figure 5.1: *The velocity profile solutions to Parker's model (top). The velocity as a function of distance.*

Type 1 starts subsonic and ends supersonic:
we keep this solution as it matches observations. It is also a critical solution, passing through the critical point when $v = c$ at which the wind becomes supersonic.

Only one set of initial conditions ($v = v_0$ at $r = r_0$) fits Type 1 and this determines the mass loss rate for the Sun (and similarly, that of other stars with similar winds). We further see that, letting $v = c$ at $r = r_c$ in Eq. 4.6 implies constant $= -3$. This gives

$$-\frac{v^2}{2c^2} + \ln\frac{v}{c} = -2\ln\frac{r}{r_c} - 2\frac{r_c}{r} + \frac{3}{2}$$

i.e.

$$\frac{v}{c}\exp\left(-\frac{v^2}{2c^2}\right) = \left(\frac{r_c}{r}\right)^2 \exp\left(-\frac{2r_c}{r} + \frac{3}{2}\right). \qquad (5.1)$$

We set $r = r_0$ at the base of the wind where the mass flow starts, so $v =$

$v_0 \ll c$ and therefore

$$\frac{v_0}{c} \approx \left(\frac{r_c}{r_0}\right)^2 \exp\left(-\frac{2r_c}{r_0} + \frac{3}{2}\right) \tag{5.2}$$

At $r \to \infty$ (and $r \gg r_c$) we have

$$\frac{v}{c} \exp\left(-\frac{v^2}{2c^2}\right) \approx \left(\frac{r_c}{r}\right)^2 \exp\left(\frac{3}{2}\right)$$

$$\text{i.e.} \quad \ln\frac{v}{c} - \frac{v^2}{2c^2} \approx -2\ln\frac{r}{r_c} + \frac{3}{2}$$

For a supersonic wind with $v \gg c$ at $r \gg r_c$ we obtain

$$\frac{v^2}{2c^2} \approx 2\ln\frac{r}{r_c} \quad \text{i.e.} \quad v \approx 2c\sqrt{\ln\frac{r}{r_c}} \tag{5.3}$$

5.2 Solar wind density profile

We find the density profile from the mass continuity equation (Eq. 4.2):

$$n \propto \frac{1}{vr^2} \propto \frac{1}{r^2\sqrt{\ln r}} \tag{5.4}$$

The density in this isothermal wind decreases to 0 at large distances, and so the pressure $p \to 0$ at $r \to \infty$. The Parker solution is consistent with our observations and with a low ISM pressure.

5.3 Stellar breeze

We come back to **Set 3** of our solutions to the velocity profile, with $v \to 0$ at $r \to \infty$. According to Eq. 4.6, we get in that case

$$-2 \ln \frac{v}{c} \approx 4 \ln \frac{r}{r_c}$$

$$\text{i.e. } \frac{v}{c} \approx \left(\frac{r_c}{r}\right)^2$$

As mass continuity says that $r^2 n v$ = constant, this yields at $r = r_c$ that $r_c^2 c n(r = r_c)$ = constant. This means that we can have a constant non-zero value for the density (and the pressure) as $r \to \infty$. Hence such stellar breeze solution cannot be confined by the ISM.

5.4 Critical radius and critical speed

All solutions are parametrised by

$$r_c = \frac{GM}{2c^2} \quad \text{and} \quad c^2 = \frac{2kT}{m_p}.$$

Taking a typical temperature for the solar corona of $T = \times 10^6$ K, the sound speed in the solar wind is $c \sim 10^5$ m s^{-1} and $r_c \approx 6R_\odot$.

So solar wind becomes supersonic for $r \gtrsim 6R_\odot$, i.e. where plasma pressure starts to dominate gravity.

5.5 Solar wind parameters

Table 1: Typical solar wind data at 1au.

	min	mean	max
$v\left(\text{km s}^{-1}\right)$	200	400	1000
$n\left(\text{m}^{-3}\right)$	4×10^{5}	6.5×10^{6}	10^{8}
$T(\text{K})$	5×10^{3}	10^{5}	10^{6}
$B(\text{T})$	2×10^{-10}	6×10^{-9}	8×10^{-8}

At the Earth, $r \simeq 215R_{\odot}$, so Eq. (32) yields

$$\frac{v}{2c}\exp\left(-\frac{v^2}{c^2}\right) = \left(\frac{10}{215}\right)^2 \exp\left(-\frac{2\times10}{215}+\frac{3}{2}\right)$$

$$\text{i.e.}\quad \frac{v}{2c}\exp\left(-\frac{v^2}{c^2}\right) = 8.91\times10^{-3}$$

This is easily solved (numerically) and gives $v \approx 3.45c \approx 345$ km s^{-1}, which agrees with observations of **slow solar wind**. Table 1 presents some typical values of the solar wind's velocity, density, temperature, and magnetic field at 1 au.

Remember: in this whole discussion of the Parker solution, we have assumed an isothermal wind. We have also assumed that there are no any other mechanism driving the solar wind (e.g. radiation pressure), and we have ignored the effects of the sun's magnetic field.

5.6 Adiabatic cooling of the solar wind

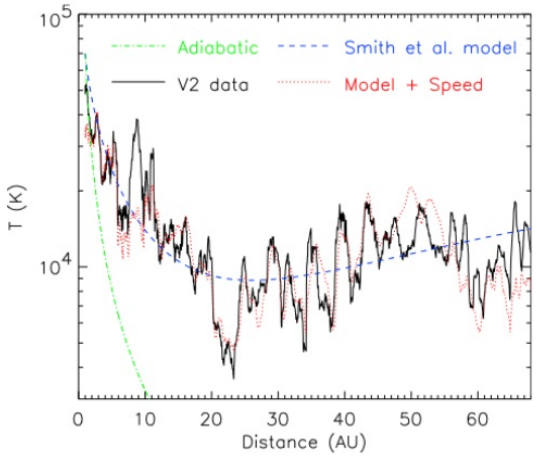


Figure 5.2: *Voyager2 temperature (solid line) versus radial distance, the adiabatic profile from Richardson & Smith, 2003*

We assumed isothermal plasma i.e. $T = \text{const}$. However, as the solar wind fills larger and larger volume, the plasma expands and cools adiabatically, i.e. $p \propto \rho^{\gamma}$ or $p \propto n^{\gamma}$. Using that $p \propto nT$, we have

$$nT \propto n^{\gamma} \quad \rightarrow \quad T \propto n^{\gamma-1}.$$

Since the density of the solar wind decreases approximately as $n(r) \propto r^{-2}$ (see Equation 5.4), the temperature decreases as

$$T(r) \propto r^{-2(\gamma-1)} \propto r^{-4/3} \qquad (5.5)$$

where we took $\gamma = 5/3$ for monoatomic hydrogen plasma.Fig 5.2 shows the departure from this law and the data require additional **heating**.

6 Observations and effects of the solar wind

LECTURE OUTLINE

- Solar wind observations
- Ram pressure
- Mass loss rate

6.1 Fast and slow solar wind

The solar wind speed at 1 au is described as **slow** and **fast** solar wind.

	V_p (km s^{-1})	B (nT)	n_p (cm^{-3})	T_p ($\times 10^5$ K)
Slow wind	380 ± 40	4.8 ± 0.7 $^{(M)}$ 3.3 ± 0.3 $^{(m)}$	7 ± 1 $^{(M)}$ 4.8 ± 0.5 $^{(m)}$	0.5 ± 0.6
Fast wind	500 ± 100	7 ± 1 $^{(M)}$ 5.6 ± 0.6 $^{(m)}$	3.5 ± 0.8 $^{(M)}$ 2.4 ± 0.2 $^{(m)}$	1.0 ± 0.8

Figure 6.1: *Typical values for the parameters of the slow and fast components of the solar wind from Larrodera & Cid, 2020(M)Maximum solar cycle. (m)Minimum solar cycle.*

6.2 Velocity of the solar wind

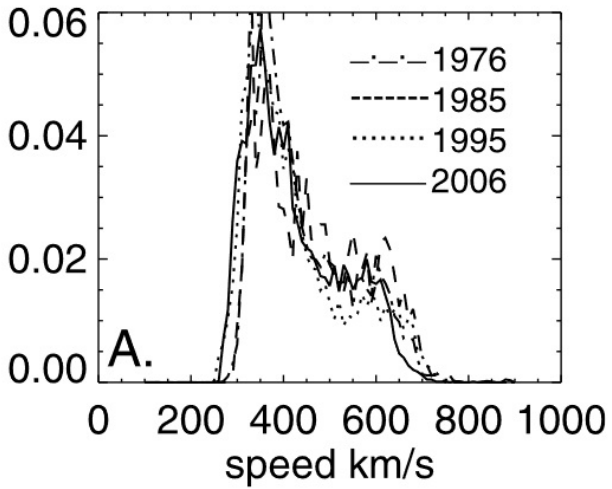


Figure 6.2: *Normalized solar wind speed distributions during solar minimum. 2006 (solid), 1995 (dotted), 1985 (dashed), and 1976 (dash-dotted). Adopted from McGregor et al, 2011*

Solar wind speed is not a constant but shows bi-modal distribution: **fast and slow** solar wind.

Slow wind speed is consistent with the speeds expected from Parker solar wind model with plasma temperature $\sim 10^6$ K.

Fast solar wind is faster than what whould be expected from Parker model.

6.3 Solar wind at different heliolatitudes

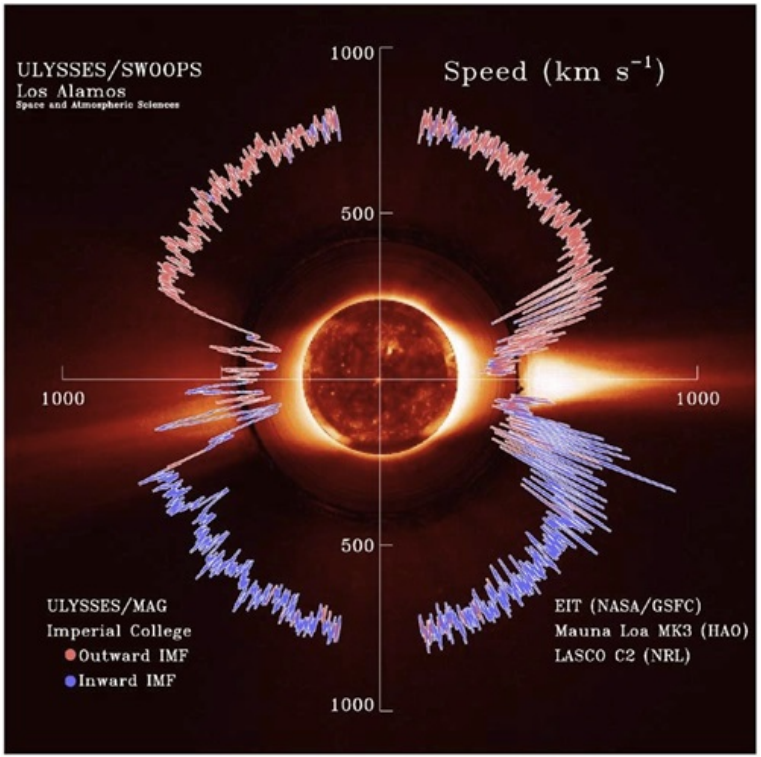


Figure 6.3: *Solar wind speed and magnetic polarity measured by Ulysses, as a function of heliolatitude, overlaid with three concentric images taken with the NASA/GSFC EIT instrument (center), the HAO Mauna Loa coronagraph (inner ring), and the NRL LASCO C2 coronagraph (outer ring). Each 1-hour averaged speed measurement has been color coded to indicate the orientation of the observed interplanetary magnetic field; red for outward pointing and blue for inward. Appeared at GRL journal cover in 1998* GRL 1998

6.4 Density profile of the solar wind

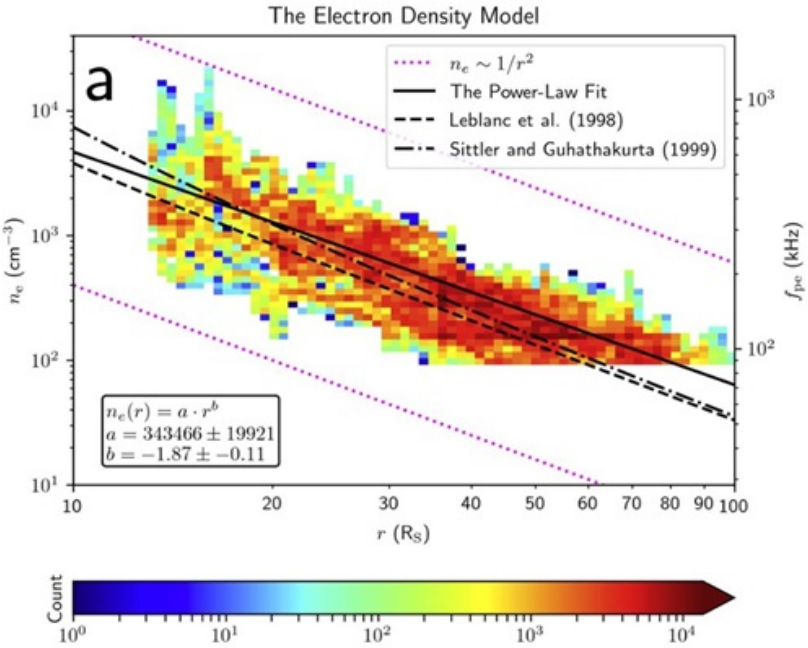


Figure 6.4: *A 2D histogram of obtained electron density as a function of radial distance from the Sun based on 2,115,146 data points obtained during the first 15 encounters by Parker Solar Probe. The power-law fit is shown as a solid black line from Kruparova et al 2023*

Recall Equation 5.4 for the plasma density in **Parker model** $n(r) \propto \frac{1}{r^2\sqrt{\ln r}}$. Profile $n(r) \propto r^{-2}$ is shown by dotted lines in Fig. 6.4.

6.5 Solar wind speed vs density and temperature

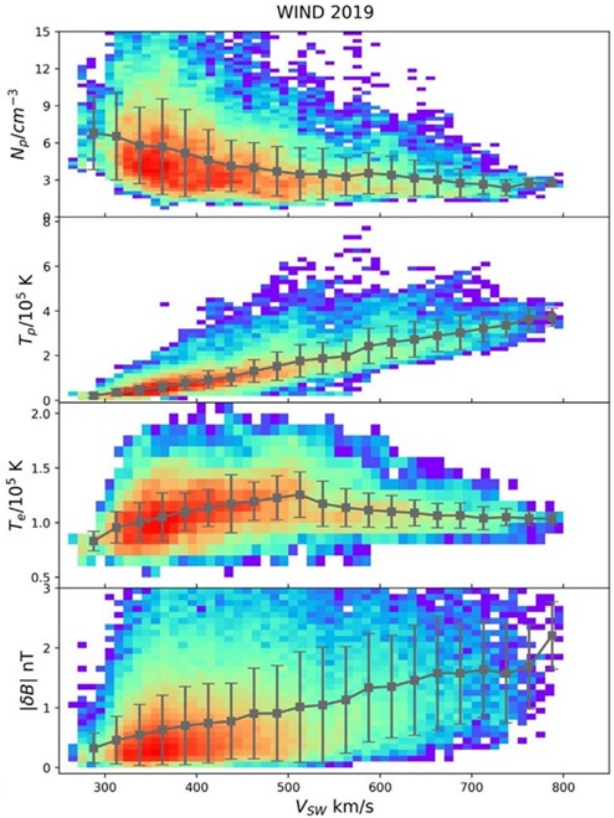


Figure 6.5: *Distributions of 1 yr (2019) of solar wind parameters measured by WIND from Shi et al 2023. From top to bottom, the proton number density N_p, the proton temperature T_p, the electron temperature T_e, and the amplitude of the magnetic field fluctuations δB as functions of the radial solar wind speed. The gray squares show the median values, while the error bars show the rms values of the binned data.*

6.6 Ram pressure

Ram pressure is a dynamic pressure due to bulk motion. It has to be distinguished from static pressure (due to thermal motions). The impact of the dynamic pressure depends on the behaviour of the wind after it hits the obstacle (i.e. other plasma of different velocity and pressure). As an example, let us consider a simple model where the wind is absorbed by the obstacle.

If we take a block (area A, size ℓ) of wind of mass $m_p n A \ell$ flowing at speed v, its momentum is given by $m_p n v A \ell$. The time needed to pass a point for this block of wind ℓ is ℓ / v. The **dynamic pressure** is the momentum absorbed per second per area and is therefore given by

$$\text{dynamic pressure} \quad = m_p n v A \ell \frac{v}{\ell} \frac{1}{A} = m_p n v^2$$

The total pressure is the sum of the static $(2nkT)$ and dynamic pressures.

The ratio between dynamic and static pressures is $\frac{m_p v^2}{2kT}$ and increases with distance. For $v = 400$ km s^{-1} and $T = 10^6$ K (i.e. temperature close to the Sun), this ratio is ~ 10.

This dynamic pressure is very important because it holds back the ISM (at $\sim$ 150 au). Indeed, ram pressure is larger than thermal pressure for distances $r \gg r_c$.

6.7 Mass loss rate

We have already seen that

$$\dot{M} = 4\pi r^2 \rho v = 4\pi r^2 n m_p v$$

For the Sun at 1 au, (take $v = 350$ km s^{-1} and $n = 3 \times 10^{-6}$ m^{-3}):

$$\dot{M} = 5 \times 10^8 \text{ kg s}^{-1}$$

How long would it take for the Sun to loose all its mass this way?

$$t = \frac{M_\odot}{\dot{M}} \approx 4 \times 10^{21} \text{ s} \approx 10^{14} \text{years}$$

With the age of the Universe of $\sim 10^{10}$ years, we see that mass loss is a negligible effect for the Sun.

This is a general result: **mass loss due to pressure-driven winds is too small to have any effect on stellar evolution.**

More generally, the mass-loss rate for pressure-driven winds is determined by the coronal density at the critical point (when the wind becomes supersonic):

$$\dot{M} = 4\pi r_c^2 c \rho_c \,,$$

with ρ_c the density at r_c.

Let us look at this more closely:

$$r_c = \frac{GM_\star}{2c^2} \quad \text{and} \quad c^2 = \frac{2kT}{m_p}$$

Hence

$$r_c = \frac{GM_\star m_p}{4kT} \propto \frac{1}{T}.$$

The position of the critical point (point at which the thermal energy is approximately the same as the gravitational potential energy) is inversely proportional to the temperature.

If T is very high (think hot stars), $r_c \approx$ stellar radius and the star will become unstable. The corresponding limit temperature for the Sun would be given by

$$T = \frac{GM_\odot m_p}{4kR_\odot} \approx 6 \times 10^6 \text{ K}$$

As long as the average coronal temperature does not exceed this value, our model should hold and the solar wind can be regarded as a pressure-driven wind.

In pressure-driven winds, r_c is many density scale-heights above the photosphere, and thus ρ_c, the density at the critical point, is not high. But what if the effective gravity acting on the wind is less, e.g. due to an onward

radiation pressure (need hot star as radiation pressure $\propto L \propto T^4$)? Then high mass loss rates will occur.

7 Radiatively driven winds

LECTURE OUTLINE

- Radiation pressure
- Eddington luminosity
- Wind velocity profile

7.1 Radiation pressure

Radiation pressure can 'loosen' the grip of gravity on the wind particles and lead to a very high mass-loss rate. We will build a simple model with the following assumptions:

- the wind is modelled as being made up of particles of mass m, photocross-section σ,
- the cross-section σ does not depend on wavelength: grey atmosphere.
- the mass flow is radial and observations are made at $r \gg R_\star$
- the wind is optically thin so that all particles can see the photosphere and are not shielded by other particles,

This latter assumption is the strongest one - close to the star where the particle density will be higher, the wind may become optically thick.

What is the outward force experienced by a wind particle due to the radiation of the star?

If our star has a **luminosity spectrum** L_λ, the number of photons N_λ emitted per second in the range between λ and $\lambda + \mathrm{d}\lambda$ is

$$N_\lambda \mathrm{d}\lambda = L_\lambda \frac{\lambda}{hc} \mathrm{d}\lambda \,,$$

where c is the speed of light and hc/λ is the photon energy. The number of such photons hitting our wind particle situated at a distance r from the star becomes

$$N_\lambda \frac{\sigma}{4\pi r^2} \mathrm{d}\lambda$$

Hence, when the photons are absorbed by the particles, the **momentum** imparted per second by these photons on our wind particle is

$$L_\lambda \frac{\lambda}{hc} \frac{\sigma}{4\pi r^2} \frac{h}{\lambda} \mathrm{d}\lambda = L_\lambda \frac{\sigma}{4\pi c r^2} \mathrm{d}\lambda$$

where $\frac{h}{\lambda}$ is the momentum of a photon.



Figure 7.1: *The star Zeta Ophiuchi (460 ly away) and its strong stellar wind compressing interstellar material NASA APOD*

Now integrate over all wavelengths and using that the bolometric luminosity is

$$L = \int L_\lambda \mathrm{d}\lambda$$

one obtains

$$\textbf{outward radiation force} = \frac{L\sigma}{4\pi c r^2}. \quad (7.1)$$

This is an inverse-square law with opposite action (direction) to that of gravity.

For example, Zeta Ophiuchi, the closest O-type star to the Sun, has a strong radiation wind (Figure 7.1)

7.2 Velocity profile

Let us balance the forces on the particle, under the assumption that for a radiatively-driven wind, the pressure term is negligible in comparison to the radiation pressure and gravity terms

$$mv\frac{\mathrm{d}v}{\mathrm{d}r} = -\frac{GM_\star m}{r^2} + \frac{L_\star \sigma}{4\pi c r^2} \tag{7.2}$$

$$mv\frac{\mathrm{d}v}{\mathrm{d}r} = \frac{GM_\star m}{r^2}(\Gamma - 1) \tag{7.3}$$

where

$$\Gamma = \frac{L_\star}{L_c} = \frac{L_\star \sigma}{4\pi G M_\star m c}$$

and

$$L_c = \frac{4\pi G M_\star m c}{\sigma}$$

is the **Eddington luminosity** and represents the point at which a star becomes radiatively unstable (when $L_\star > L_c$).

By integrating Eq. 7.3, we get a solution for the wind speed:

$$\frac{1}{2}v^2 = \frac{1}{2}v_0^2 + GM_\star(\Gamma - 1)\left(\frac{1}{R_\star} - \frac{1}{r}\right)$$

If we let $v_0 = 0$ (null wind speed at the stellar surface $r = R_\star$), we obtain

$$v(r) = v_\infty \left(1 - \frac{R_\star}{r}\right)^{1/2}, \tag{7.4}$$

where

$$v_\infty = \left[\frac{2GM_\star}{R_\star}(\Gamma - 1)\right]^{1/2} = v_{\rm esc}\sqrt{\frac{L_\star}{L_c} - 1} \tag{7.5}$$

This is the **Castor, Abbot, Klein (CAK) velocity profile.**[10]. Recall here that the escape velocity is given by

$$v_{\rm esc}^2 = \frac{2GM}{R}$$

[10] See here for the original paper in ApJ,1975

Remarks:

If $L_\star > L_c$ (i.e. $\Gamma > 1$) - as for a radiatively-driven wind - radiation wins and mass is lost.

If $L_\star < L_c$ (i.e. $\Gamma < 1$) gravity wins and mass is accreted.

If $L_\star \gg L_c$, the terminal velocity is $v_\infty \approx \sqrt{\frac{\sigma L_\star}{2\pi R_\star mc}}$. This can also be written as

$$v_\infty \approx 10 \text{ km s}^{-1} \left(\frac{\sigma}{\sigma_T}\right)^{1/2} \left(\frac{m_p}{m}\right)^{1/2} \left(\frac{L_\star}{L_\odot}\right)^{1/2} \left(\frac{R_\odot}{R_\star}\right)^{1/2}$$

Radiatively-driven winds are found in early-type stars (OB) with high luminosities (see e.g. Fig. 7.1).

7.3 Mass-loss rate

We further assume that each photon interacts just once with wind particles. The momentum due to the star's luminosity per second is $L_\star/c$. The final momentum of the wind per second is given by $\dot{M}v_\infty$. Therefore,

$$\dot{M} = \frac{L_\star}{cv_\infty} \tag{7.6}$$

Taking data for a star such as ζ Puppis $\left(L_\star \approx 10^6 L_\odot \text{ and } v_\infty \approx 2700 \text{ km s}^{-1}\right)$, we get $\dot{M} \approx 4.9 \times 10^{17}$ kg s^{-1}. This is huge, many orders of magnitude larger than our Sun's mass-loss rate!

7.4 Stellar wind luminosity

The amount of kinetic energy imparted to the wind per second is:

$$L_w = \frac{1}{2}\dot{M}v_\infty^2$$

Using the expression for $\dot{M}$ (Eq. 7.6), one obtains

$$L_w = \frac{1}{2}\frac{v_\infty}{c}L_\star$$

Typically, $L_w \approx L_\star/200$: most of the energy is lost via radiation.

7.5 Complications

Firstly, taking the mass-continuity equation yields

$$\rho v = \frac{\dot{M}}{4\pi r^2}.$$

This means that v cannot be zero at $r = R_\star$ unless the density there $\rho \to \infty$. In practice, the whole outer layer of the star is slowly moving outwards.

Secondly, the star is not a point-source, so the radiation pressure close in is not proportional to $1/r^2$. The non-radial photons give an oblique kick and reduce the radiation pressure of nearby particles. Let us try to work out how much reduction (Fig. 7.2). Let dI be the energy flux of a source of intensity

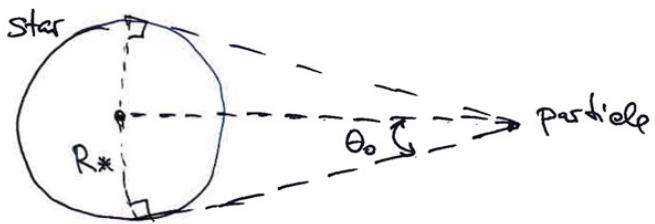


Figure 7.2: *Diagram showing how much of the star's surface is seen by a wind particle close to the star. θ_0 denotes the maximum angle to the edge of the star.*

I from a solid angle $\mathrm{d}\Omega$: $\mathrm{d}I = I\cos\theta\mathrm{d}\Omega$. The momentum per second through unit area is $\mathrm{d}I/c$ and to calculate in the radial direction is to multiply by $\cos\theta$

$$\frac{\mathrm{d}I}{c}\cos\theta = \frac{I}{c}\cos^2\theta\mathrm{d}\Omega$$

Therefore, the total pressure from the star is

$$P = \frac{I}{c}\int_0^{\theta_0} 2\pi\cos^2\theta\sin\theta\mathrm{d}\theta = \frac{2\pi}{3}\frac{I}{c}\left(1-\cos^3\theta_0\right)$$

By geometry,

$$\cos\theta_0 = \left(1-\left(\frac{R_\star}{r}\right)^2\right)^{1/2}.$$

While for a blackbody we have $I = \sigma_{SB}T^4/\pi$, with σ_{SB} is the Stefan-Boltzmann constant.

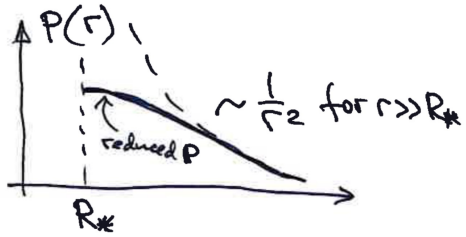


Figure 7.3: *Diagram showing two regimes for how much pressure is received from the star close to it, and further away.*

Finally,

$$P = \frac{2}{3}\frac{\sigma}{c}T^4\left[1-\left(1-\left(\frac{R_\star}{r}\right)^2\right)^{3/2}\right]$$

Figure 7.3 shows how the pressure varies with distance to the star. Note that

- even if $L > L_c$, gravity can accrete material that is close to the star;
- we have assumed photon absorption;
- the effect of a finite star size could increase v_∞ by a factor ~ 2.

Thirdly, the atmosphere is not grey. The scattering cross-section σ depends on wavelength, and is dominated by the effects of heavy ions in the star's atmosphere, which have large resonant absorptions. These give **line-driven winds**.

8 Observed line profiles: P-Cygni profiles

LECTURE OUTLINE

- The formation of spectral lines in stellar winds
- Multiple scattering

8.1 Resonant lines

Winds with strong resonant lines (**line-driven winds**) exhibit characteristic profiles (Fig. 8.1) called **P-Cygni profiles**, named after the P-Cygni star. These profiles are an important diagnostic of wind structure, and are clearest when there is lots of resonant scattering.

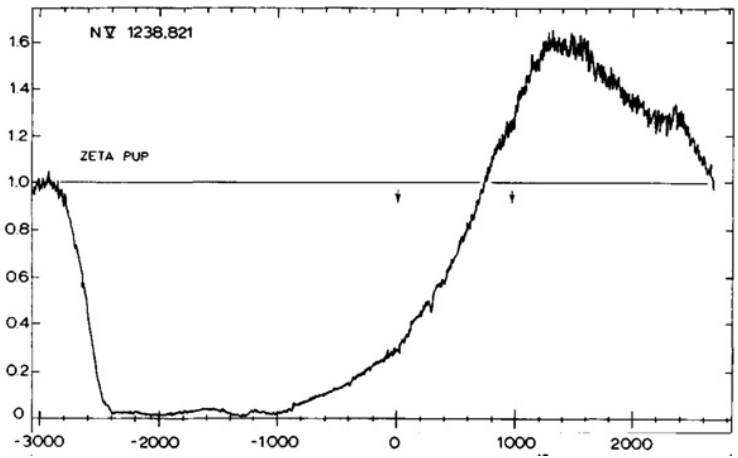


Figure 8.1: *The P Cygni profiles in the spectrum of ζ Pup. The rest wavelengths are indicated by small arrows; velocities are in km/s.*

8.2 P-Cygni profile: qualitative approach

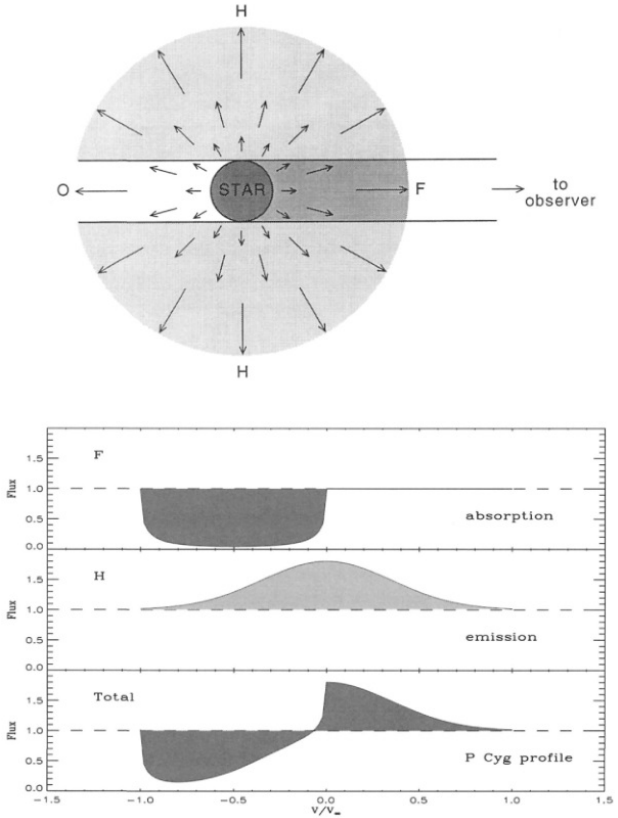


Figure 8.2: *Figure shows the contribution of the different regions of a wind to the flux that gives rise to a P Cygni profile. The star S emits a continuum with a photospheric absorption line. The region F in front of the star scatters radiation from the star, that would have reached the observer if there were no wind, out of the line of sight to the observer. This removal of photons produces a blue shifted absorption component. The halo H scatters radiation from the photosphere in all directions. Some of this radiation is sent in the direction of the observer. the contributions from the star (the continuum) with the absorption from F and the emission from H. The P Cygni profile is the sum of these three contributions.*

8.3 Absorption/emission in a shell

Take a strong line of rest wavelength λ_0 and a shell of plasma around the star at radius r, expanding at velocity $v(r)$. As discussed earlier, the photons from the star may be scattered by the atoms / ions in the plasma who see them with a Doppler shift proportional to v. This broadens the line profile.

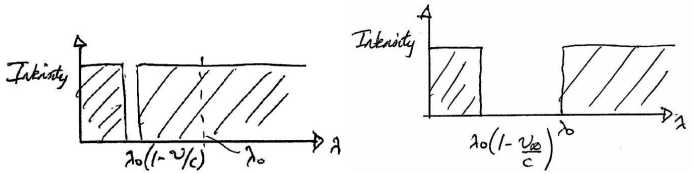


Figure 8.3: *Left: Schematic diagram showing the absorption feature in the star's spectrum due to photons being scattered out of the line of sight by the moving shell. Right: Overall picture with outermost shells moving at v_∞.*

If that was the only mechanism taking place, we would observe an abrupt absorption feature (shown schematically in Fig. 8.3) where the dip in intensity is due to photons being scattered out of the line of sight by the part of the shell in front of the star. If the outermost shells have a maximum expansion speed of v_∞, the overall (still schematic) picture would be that on the right panel of Fig. 8.3. The missing emission between

$\lambda_0 (1 - v_\infty/c)$ and λ_0 is a broad absorption feature to the blue side (i.e. at wavelengths shorter than λ_0) of the line profile.

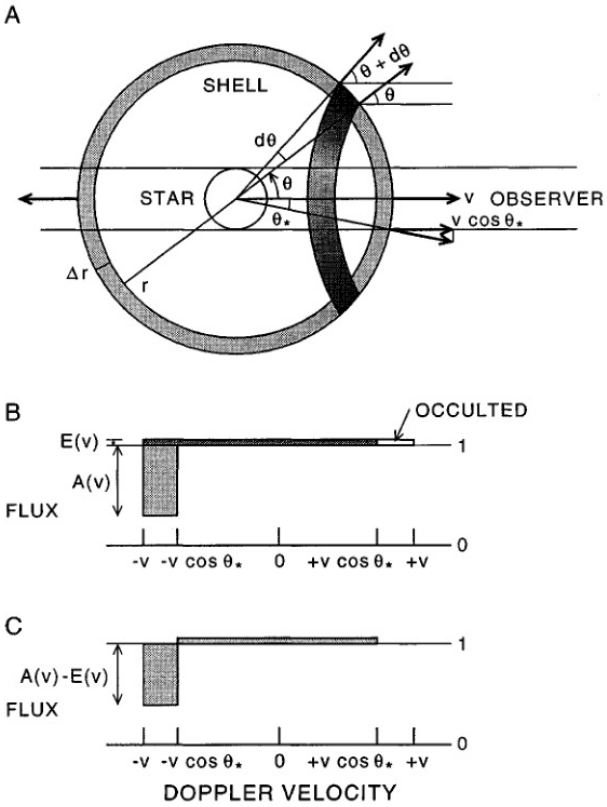


Figure 8.4: *The profile of a thin scattering shell. A: the geometry of the shell. B: the resulting absorption, A(v), and the flat emission E(v). Part of this emission is occulted by the star. C: the resulting profile is the sum of the absorption and the emisson.*

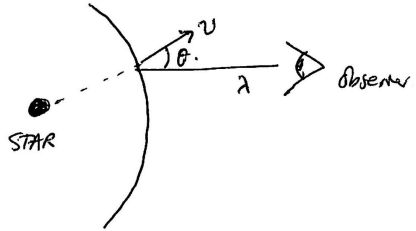


Figure 8.5: *Photons emitted in other directions can be scattered into the observer's line of sight.*

Another process needs to be incorporated to fully explain the overall shape of P-Cygni profiles. Photons can also be scattered from other regions into our line of sight. Photons emitted at a wavelength of λ_0 in the wind shell's rest frame are observed by us at a wavelength of $\lambda_0 \left(1 - \frac{v}{c} \cos\theta\right)$ (see Fig. 8.5). This means that we are now getting more photons than in the surrounding continuum region, therefore there appears an emission feature in the line profile (see Fig. 8.4) due to the scattering from that shell. However, there are many shells, and their contributions will add up in a manner shown schematically by Fig. 8.6.

The overall profile is the result of the absorption and emission mechanisms discussed above, shown in Fig. 8.6. It is widely observed in stars with line-driven winds, of which P-Cygni is the canonical example.

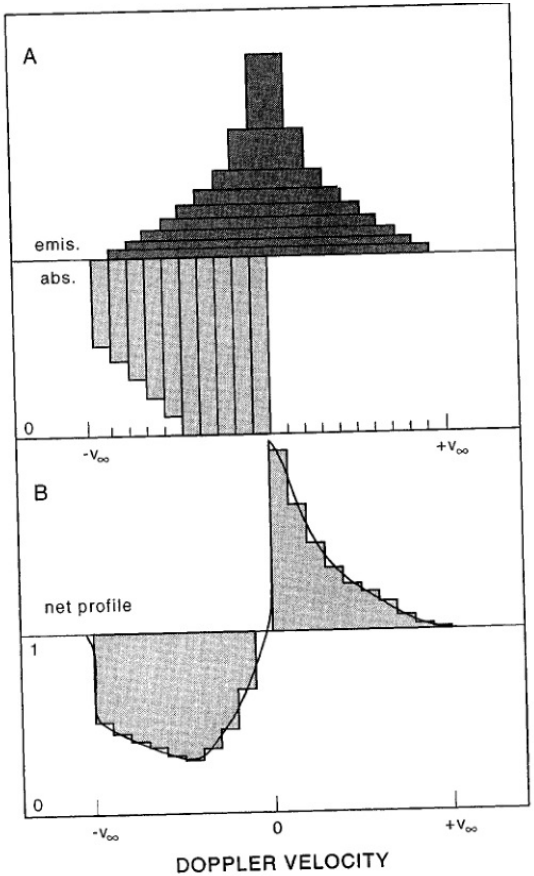


Figure 8.6: *The profile of a scattering line in a wind with outward increasing velocity. Upper figure: the separate contributions of shells consist of narrow absorptions and flat wide emissions. Lower figure: the resulting P Cygni profile is the sum of all the contributions.*

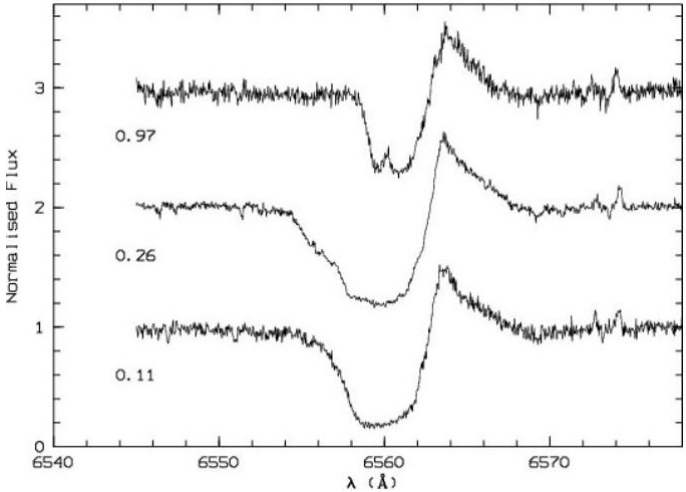


Figure 8.7: *The observed P-Cygni profile of* Hα *in star IRAS 08544-4431 (evolved star in binary system surrounded by a dusty disc) varies with time. Its strength reveals a fast stellar wind. From Maas et al, A&A, (2003).*

It is interesting to note that for stars with substantial accretion discs, the **inverse P-Cygni profile** can be observed. An example of such star is a star of the T-Tauri type (young protostars that are still undergoing gravitational collapse). In fact, these unstable stars show line profiles that can switch between the two types over very short time periods (a few days).

8.4 Scattering

Photon scattering must be considered carefully when considering conservation of momentum and of energy. Let us do this in the case where wind particles are accelerated to non-relativistic speeds:

$$\text{Convervation of momentum: } \hbar k = mv \tag{8.1}$$

$$\text{Convervation of energy: } \hbar\omega = \frac{1}{2}mv^2 \tag{8.2}$$

Dividing Eq. 8.2 by 8.1 gives $v = 2c$. This can't work, so we've missed something. Perhaps the particle is in some excited state, with internal energy U, in which case Eq. 8.2 would become $\hbar\omega = \frac{1}{2}mv^2 + U$. Or the particle radiates some of the energy absorbed (though there would not be any kick to the particle if the energy absorbed was entirely radiated isotropically).

However, a key point is that if all particles (photons and ions) have moments

$\vec{p}_i$, then conservation of momentum says that

$$\sum_i \vec{\mathbf{p}}_\mathbf{i} = \text{const}$$

but $\sum_i |\vec{\mathbf{p}}_i|$[11] can increase rapidly with multiple scattering.

In practice, in a stellar wind where multiple scattering is important, the terminal velocity is often underestimated by the single-scattering argument. Even if photons loose energy (and therefore are redshifted) after each scatter, they can still impart momentum to wind particles multiple times. Therefore we should rewrite Eq. 7.6 as

$$\dot{M} = \eta \frac{L}{c v_\infty},$$

with η a performance factor with typical values of $\sim 5 - 50$ in Wolf-Rayet stars (where multiple scattering is the norm).

[11] Here the sums are carried over all particles.

8.5 Multiple scattering

In equation 7.3, we assumed single absorption with cross-section σ. Let us multiply Eq. 7.2 by $4\pi r^2 n$ and ignore gravity (i.e. radiation pressure dominates):

$$4\pi r^2 n m v \frac{\mathrm{d}v}{\mathrm{d}r} = \frac{L_\star \sigma 4\pi r^2 n}{4\pi c r^2} \tag{8.3}$$

noting that $\dot{M} = const = 4\pi r^2 n m v$ and integrating we find

$$\dot{M} v_\infty = \frac{L_\star}{c} \int_{R_\star}^{\infty} \sigma n dr = \frac{L_\star}{c} \tau \tag{8.4}$$

where τ is the optical depth. This might be a problem when $\tau \to \infty$. However, at maximum, all of the radiative energy of the star is transferred to the wind, so $\dot{M} v_\infty^2/2 < L_\star$ or $\tau < 2c/v_\infty$ or

$$v_\infty < \sqrt{2L_\star/\dot{M}}.$$

8.6 Driver mechanisms

Let us summarise the different types of winds discussed so far, and give a brief description of other types of winds that have been studied:

- **Coronal (pressure-driven) winds** driven by gas pressure from a hot corona. The solar wind is a typical example. They generally yield small mass-loss rates.
- **Dust-driven (radiation-driven) winds**: radiation supplies the force to the dust which is a good absorber of continuum radiation. Practically, dust in the outer envelopes of cool stars drags the plasma out with it.
- **Line-driven (radiation-driven) winds**: radiation pressure is exerted via absorption and scattering of photons in strong resonant spectral lines. The magnitude of the effect depends on the velocity profile and the magnitude of the Doppler shift.

- **Pulsation-driven winds** are found in cool variable stars (e.g. Mira) which pulsate radially and throw off their outer layers. These layers may subsequently fall back (in part) towards the star under the action of gravity, but overall they will be dispersed over several consecutive pulsations.
- **Magnetically-driven winds**: when plasma flows along magnetic field lines. This results in Alfvén waves travelling along the field lines at the Alfvén speed.
- **Magnetically-rotating winds**: when plasma flows along magnetic field lines and is flung out by the rotation of the star.

The next section will discuss the important role played by the magnetic field in the solar wind.

9 Magnetic solar atmosphere

LECTURE OUTLINE

- Frozen-in magnetic field
- Magnetic pressure
- Plasma beta

9.1 Role of the magnetic field



Figure 9.1: *Solar corona during the total solar eclipse that occurred in April of 2023. NASA APOD*

The dynamic structure of the solar atmosphere (and solar wind) depends strongly on the magnetic field linked through the plasma (Figure 9.1). Let us take a look at two important properties.

9.2 Magnetic field in moving plasma

We consider a region of plasma moving with bulk velocity $\vec{\mathbf{v}}$ and immersed in a magnetic field (sounds like we are talking about the solar wind itself!). We want to know how the magnetic flux changes through some area that moves with the plasma. To answer this, we need Maxwell's equations, and we will work in the co-moving frame of the plasma.

Maxwell-Faraday law: A circulating electric field is produced by a magnetic field that changes with time.

$$\nabla \times \vec{\mathbf{E}} = -\frac{\partial \vec{\mathbf{B}}}{\partial t} \tag{9.1}$$

Since there is an electric field produced, there is also a circulating current produced. This brings us to **Ohm's law**.

9.3 Ohm's law

If the plasma (conductor) is moving, this creates an extra term added to the induced current by the Lorentz force on the charge carriers.

$$\vec{\mathbf{j}} = \sigma(\vec{\mathbf{E}} + \vec{\mathbf{v}} \times \vec{\mathbf{B}}), \tag{9.2}$$

with $\vec{\mathbf{j}}$ the current density, and $\sigma = 1/\eta$ the electrical conductivity, and η is the resistivity. Therefore, rewriting for $\vec{\mathbf{E}}$

$$\vec{\mathbf{v}} \times \vec{\mathbf{B}} - \frac{\vec{\mathbf{j}}}{\sigma} = -\vec{\mathbf{E}}$$

$$\nabla \times \left(\vec{\mathbf{v}} \times \vec{\mathbf{B}} - \frac{\vec{\mathbf{j}}}{\sigma} \right) = -\nabla \times \vec{\mathbf{E}} = \frac{\partial \vec{\mathbf{B}}}{\partial t}$$

Solar observations suggest that the electrical conductivity is very high, hence we can ignore the $\vec{\mathbf{j}}/\sigma$ term. Hence

$$\nabla \times (\vec{\mathbf{v}} \times \vec{\mathbf{B}}) = \frac{\partial \vec{\mathbf{B}}}{\partial t} \tag{9.3}$$

9.4 Lenz law

It is linked to Maxwell-Faraday law and states that *currents induced by changing* ***magnetic flux*** *always flow in the direction so as to oppose the change in flux*, where magnetic flux is

$$\text{magnetic flux:} \quad \Phi = \int_S \vec{\mathbf{B}} \cdot \overrightarrow{dS} \tag{9.4}$$

One consequence of this is that we expect to change the direction of the circulating induced current if we reverse the direction in which the magnetic field moves (or the direction of bulk motion of the plasma through the magnetic field).

So, what happens in the solar atmosphere?

9.5 Magnetic flux

There are two components to the changing magnetic flux

$$\frac{d\Phi}{dt} = \frac{d}{dt}\int_S \vec{\mathbf{B}} \cdot \overrightarrow{dS}$$

External changes in $\vec{\mathbf{B}}$: these are determined by the double integral below

$$\int_S \frac{\partial \vec{\mathbf{B}}}{\partial t} \cdot \overrightarrow{dS}$$

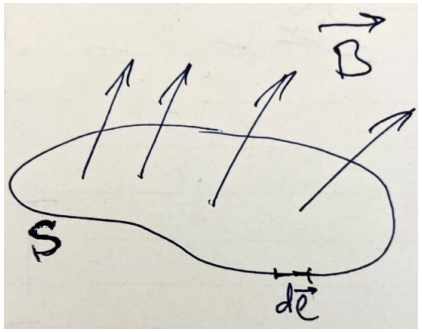


Figure 9.2: *Magnetic field through the area S.*

where S is the area through which the magnetic flux is evaluated.

Extra induced electric field due to the fact that the plasma is moving:

$$-\oint_{\text{loop}} (\vec{\mathbf{v}} \times \vec{\mathbf{B}}) \cdot d\vec{\mathbf{l}}$$

This closed integral is over the loop enclosing the surface $\vec{\mathbf{S}}$, and $d\vec{\mathbf{l}}$ is a length element over that loop (Fig. 9.2). The minus sign is expected here as we're considering the induced electric field this arises from **Lenz law**.

These are the only two components to the changing magnetic flux, as we have decided to ignore the $\vec{\mathbf{j}}/\sigma$ term due to the very high conductivity.

Now the changing magnetic flux is given by the ordinary differential w.r.t. time of the magnetic field $\vec{\mathbf{B}}$ through some surface $\vec{\mathbf{S}}$. Therefore,

$$\frac{d}{dt}\int_S \vec{\mathbf{B}}\cdot\overrightarrow{dS} = \int_S \frac{\partial\vec{\mathbf{B}}}{\partial t}\cdot\overrightarrow{dS} - \oint_{\text{loop}} (\vec{\mathbf{v}}\times\vec{\mathbf{B}})\cdot d\vec{\mathbf{l}}$$

By Stoke's law:

$$\oint_{\text{loop}} (\vec{\mathbf{v}}\times\vec{\mathbf{B}})\cdot d\vec{\mathbf{l}} = \int_S \nabla\times(\vec{\mathbf{v}}\times\vec{\mathbf{B}})\cdot\overrightarrow{dS}$$

And for large values of σ

$$\int_S \nabla \times (\vec{\mathbf{v}} \times \vec{\mathbf{B}}) \cdot \overrightarrow{dS} = \int_S \frac{\partial \vec{\mathbf{B}}}{\partial t} \cdot \overrightarrow{dS}$$

Hence, the overall result is

$$\frac{d}{dt} \int_S \vec{\mathbf{B}} \cdot \overrightarrow{dS} = 0 \tag{9.5}$$

The magnetic flux through the area enclosed by the loop is constant as the loop deforms, so long as the conductivity σ is high. This is flux freezing: **the magnetic field and the plasma are "frozen" together.**

9.6 Frozen-in magnetic field

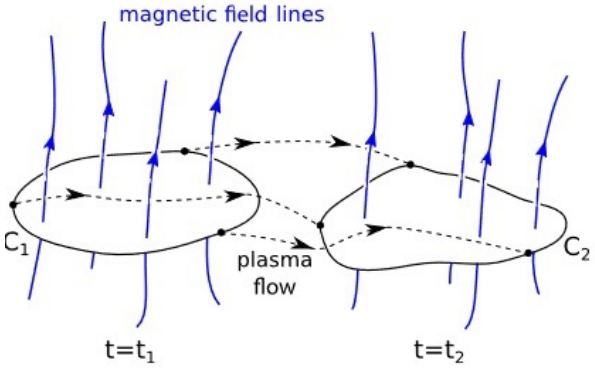


Figure 9.3: *Magnetic flux conservation: the flux through a curve C_1 at time t_1 remains constant when it is distorted into a curve C_2 at time t_2 by a plasma motion from Priest, 2022*

Alfven's or the frozen-in flux theorem states that "in a fluid with infinite electric conductivity, the magnetic field is frozen into the fluid and has to move along with it". How does this affect the plasma dynamics? Plasma in general has very low resistivity $1/\sigma$ (that inhibit electric fields). When σ is large, the magnetic field, and the plasma, are "stuck" to each other. If the plasma moves, so do the magnetic field lines and vice versa (Figure 9.3). The field lines are similar to elastic bands that want to be as straight as possible. So, the field lines will exert a force (called the tension force) on the plasma to move it. Or, the magnetic field is frozen into the plasma.

9.7 Magnetic pressure

Ampere-Maxwell's law tells us that currents travelling in opposite directions produce a repulsive force, while currents travelling in the same direction produce an attractive force. Hence a magnetic flux tube will experience inward / outward pressures of magnitude

$$P = \frac{B^2}{2\mu_0},$$

where μ_0 is the permeability of vacuum. Because the field is frozen in the plasma, the plasma flow is affected too. The relationship between the plasma and the magnetic field depends on the ratio between the gas pressure and the magnetic pressure, and we introduce a dimensionless parameter β,

$$\textbf{plasma beta:} \quad \beta = \frac{2\mu_0 nkT}{B^2} \tag{9.6}$$

called **plasma beta** to distinguish possible cases:

Two regimes:

$\beta \ll 1$: magnetic field dictates how the plasma moves. This regime applies to the solar corona (or inside coronal loops, for instance as in Figure 9.4).

$\beta \gg 1$: the plasma dominates and plasma motions distort the magnetic field. This regime applies to the solar wind far from the Sun, e.g. near 1 au or near solar photosphere (Figure 9.5).

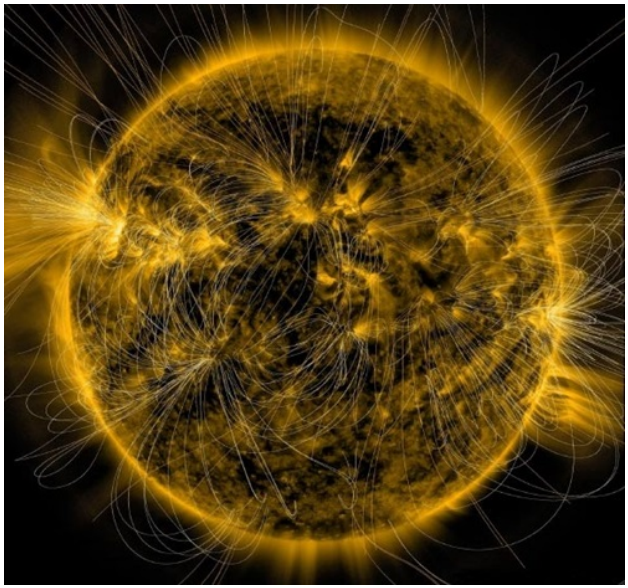


Figure 9.4: *EUV image of the Sun with magnetic field lines (white) over-plotted from NASA SDO*

In the Sun's case, the value of β increases slowly. In the corona ($\beta \ll 1$), the plasma streams along the magnetic field lines (loop structures, see Figure 9.6). Close to the Earth ($\beta \gtrsim 1$), the magnetic field acts as a tracer of where the plasma is.

9.8 Variation of plasma beta with height

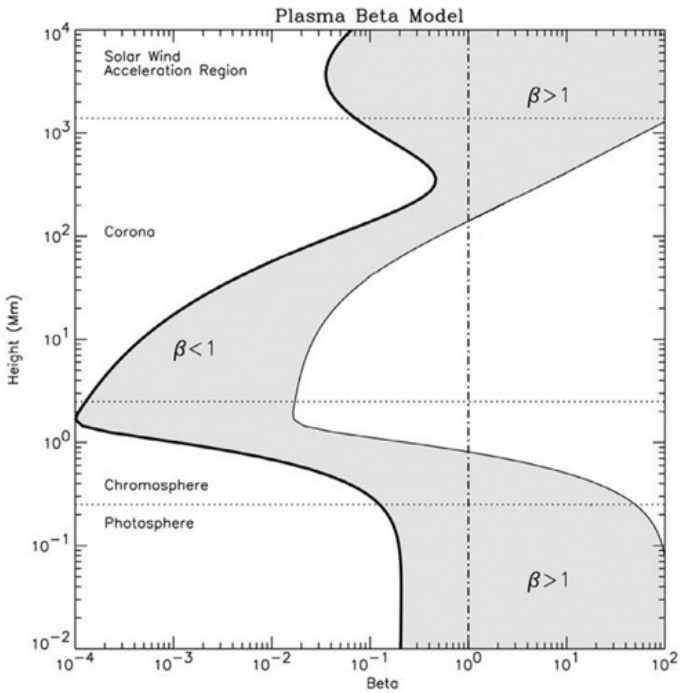


Figure 9.5: *Plasma beta depending on the height in the solar atmosphere. Adopted from Gary (2001).*

The region $\beta \ll 1$ is sandwiched between two regions which have $\beta \gg 1$. Figure 9.5 shows plasma beta model over an active region. The plasma beta as a function of height is shown shaded for open and closed field lines originating between a sunspot (large B) and a plage region of weaker B.

9.9 Solar magnetic field cartoon

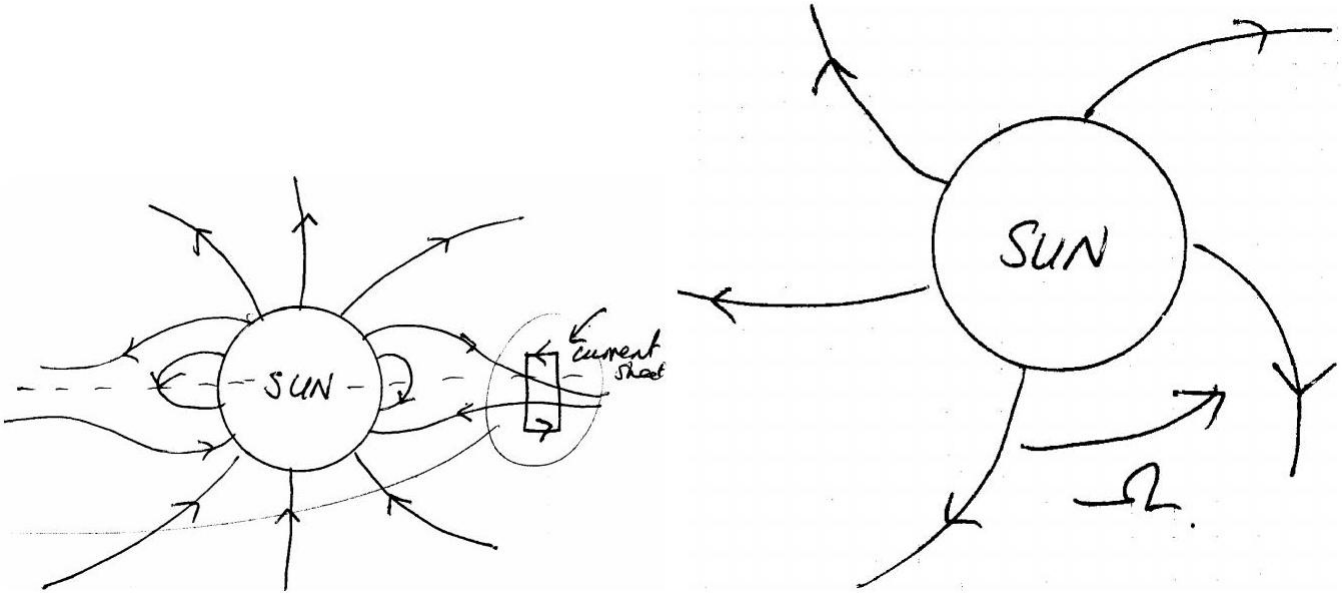


Figure 9.6: *Left: A view of the Sun seen edge-on, showing open and closed field regions. Right: A view of the Sun from above the pole. Only open field lines are shown here.*

10 The effects of magnetic field

LECTURE OUTLINE

- Solar rotation and solar wind
- Parker spiral
- Magnetic activity

10.1 Solar cycle variation of solar wind

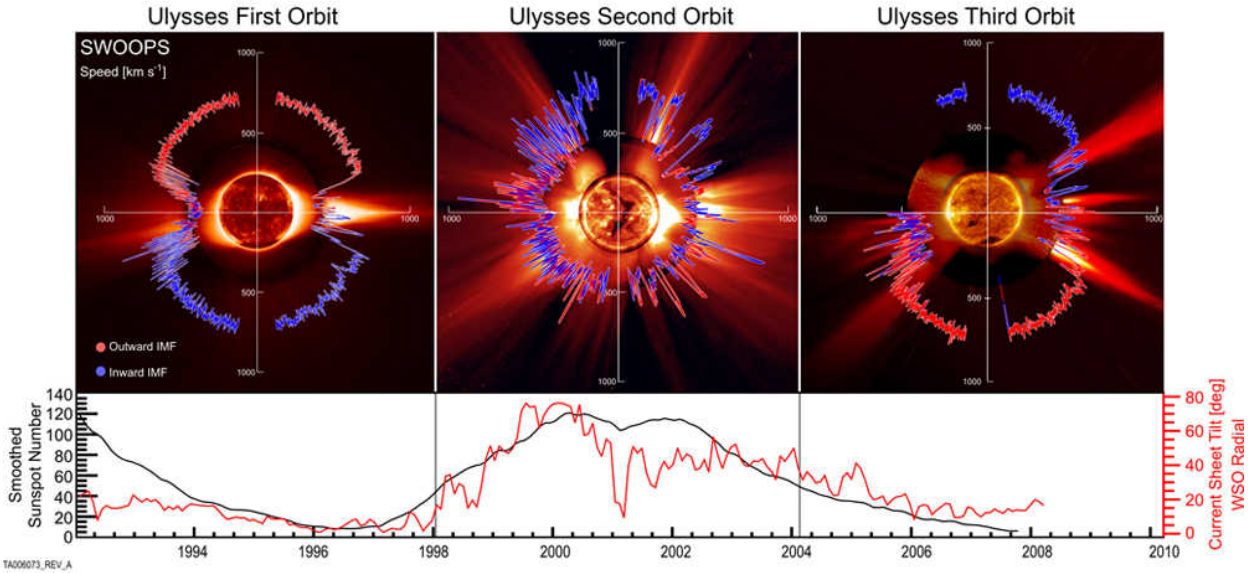


Figure 10.1: *Radial plots of the solar wind speed observed in Ulysses polar orbits of the Sun, each of which take six years to complete. The blue colored lines represent the outward interplanetary magnetic field; the red colored lines the inward IMF. From NASA/Ulysses*

10.2 Sun's influence on the environment in space

The Sun's influence on the environment in space finds its origin in three broad mechanisms (modulated by the 11-year solar cycle):

1. fast solar wind: high-speed streams $\left(v \approx 600 \text{ km s}^{-1} \text{ at } 1\text{au}\right)$ coming from coronal holes,
2. slow solar wind: coming from edges of active regions and coronal streamers,
3. high-speed transients (ejecta) associated with **solar flares** and **coronal mass ejections**.

These have different velocities: when higher-speed bulk flows catch up with slower ones, we observe compressed leading edges of higher plasma density and magnetic field intensity.

Space weather: Magnetic fields, plasma, energetic particles ejected from the Sun interact with the Earth's magnetosphere/atmosphere and produce a number of effects. Metoffice/space weather

Variability of the solar atmosphere

As the magnetic fields change at different time scales, so the atmosphere of the Sun changes:

Every 11 years or so, the Sun's magnetic field completely flips.

Solar rotation (approximately 27 days)

Active regions, equatorial coronal holes (approximately days/weeks)

Transient phenomena (flares and coronal mass ejections, hours)

10.3 Solar flares and coronal mass ejections



Figure 10.2: *Solar flare and coronal mass ejection. The expanding bubble of hot plasma expands into SOHO-LASCO C3 field of view. from NASA/GSFC*

10.4 Magnetic reconnection

Magnetic reconnection is believed to power solar flares and coronal mass ejections. The magnetic topology is rearranged and magnetic energy is converted to kinetic energy, thermal energy, and particle acceleration.

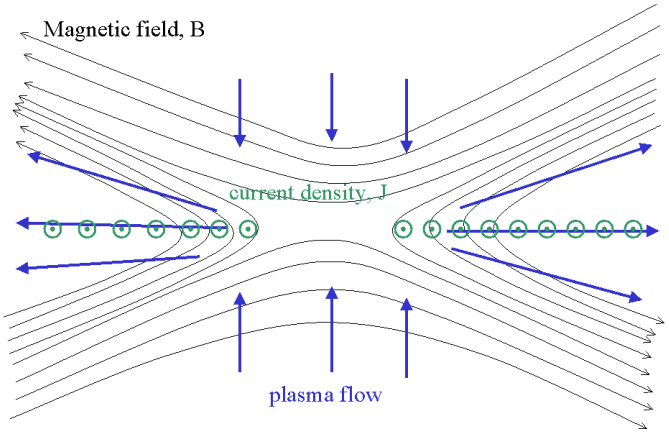


Figure 10.3: *Illustration of magnetic reconnection of oppositely directed magnetic lines.*

Magnetic reconnection is a breakdown of Alfvén's theorem ("frozen-in flux theorem") near neutral point/layer Sweet, 1958. Resistivity is high in the thin layer called current sheet (magnetic diffusion) region. However, the details of solar flares and coronal mass ejections are still poorly understood.

10.5 Solar rotation and Parker spiral

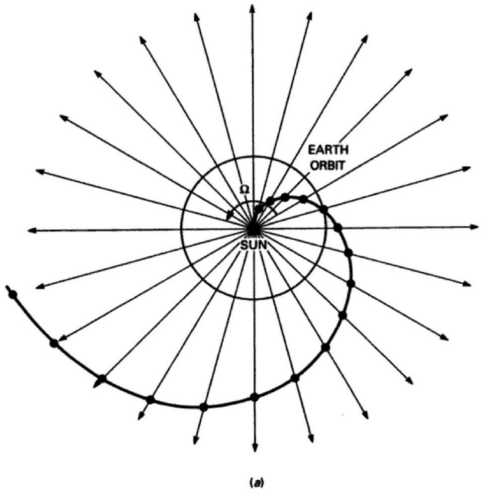


Figure 10.4: *Diagram showing how the magnetic field of the solar wind takes up its spiral shape. The plasma leaving the corona moves radially to start with, and the magnetic field is dragged with it. The dynamics of the plasma associated with one field lines is shown here while the Sun rotates. From Longair (Chapter 11)*

The left panel of Fig. 9.6 shows the Sun seen edge on (observer in the ecliptic plane). Open and closed magnetic field lines are represented. All lines have both feet anchored on the Sun.

- open field lines extend to very large distances. Coronal holes (regions of lower plasma density) are found in these open field regions. The

fast solar wind originates from these regions.

- closed field lines confine the plasma to comparatively higher densities.
- current sheets are formed above the cusp of coronal streamers. In these (induced) current sheets, $\oint \vec{\mathbf{B}} \cdot d\vec{\mathbf{l}} \neq 0$.

All of these structures rotate with the Sun. The right panel of Fig. 9.6 shows a view from above the pole of the Sun. The rotating Sun gives an overall **spiral shape** to open field lines along which the outflowing plasma is channelled (Fig. 10.4).

10.6 Solar wind magnetic field

In the coordinate system rotating with the Sun (solar equator at $\theta = \pi/2$), the velocity components of the solar wind velocity can be written Lecture notes):

$$\begin{aligned} v_r &= v, \\ v_\theta &= 0, \\ v_\phi &= -\Omega r \sin\theta, \end{aligned} \tag{10.1}$$

where $\Omega \simeq 2\pi/(27 \text{ days}) \simeq 2.7 \times 10^{-6}$rad/sec is the angular velocity. The radial component is unchanged, but the azimuthal velocity u_ϕ appears due to the transformation to the rotating frame of reference and the velocity field lines should satisfy the differential equations at constant θ.

$$\frac{dr}{v_r} = \frac{r \sin\theta d\phi}{v_\phi} \tag{10.2}$$

Substituting 10.1 into 10.2, and $v_r = \text{const} = v_{sw}$ [12], one finds

$$dr = -\frac{v_{sw}}{\Omega} d\phi \quad \Rightarrow \quad r - r_0 = -\frac{v_{sw}}{\Omega}(\phi - \phi_0) \tag{10.3}$$

where the field-lines pass through the point (r_0, θ, ϕ_0). The spherically symmetric (in Sun's frame) magnetic field satisfying $\nabla \vec{\mathbf{B}} = 0$ dragged by the plasma creates a spiral with the magnetic field lines given by 10.3 and the following expressions for the components of the interplanetary magnetic field (Parker,1958):

$$\begin{aligned} B_r(r, \theta, \phi) &= B(r_0, \theta, \phi_0)\left(\frac{r_0}{r}\right)^2, \\ B_\theta(r, \theta, \phi) &= 0, \\ B_\phi(r, \theta, \phi) &= -B(r_0, \theta, \phi_0)\frac{\Omega(r - r_0)}{v_{sw}}\frac{r_0^2}{r^2}\sin\theta. \end{aligned} \tag{10.4}$$

[12] which is a good approximation for $r \gg r_c$ - see lecture on Parker solar wind

which is the same in the stationary lab frame.[13]. Hence, the magnetic field-lines of the Sun are drawn into **Archimedean spirals** by the solar rotation. Figure 10.5 shows that the angle depends on the solar wind speed (fast wind is more radial).

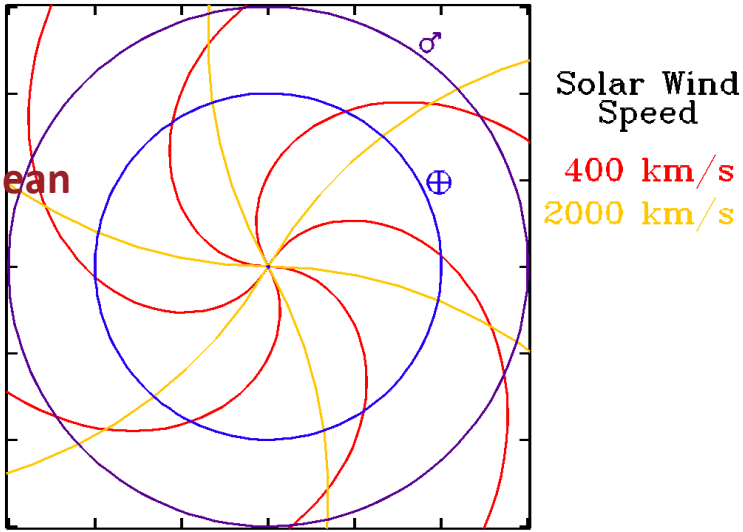


Figure 10.5: *The Parker spiral structure of the average interplanetary magnetic field, shown in the solar equatorial plane for two solar wind speeds, 400 km/s and 2000 km/s. The field is approximately* 45° *from the radial direction at 1 au.*

[13] with additional electric field

10.7 Observation of magnetic field in the heliosphere

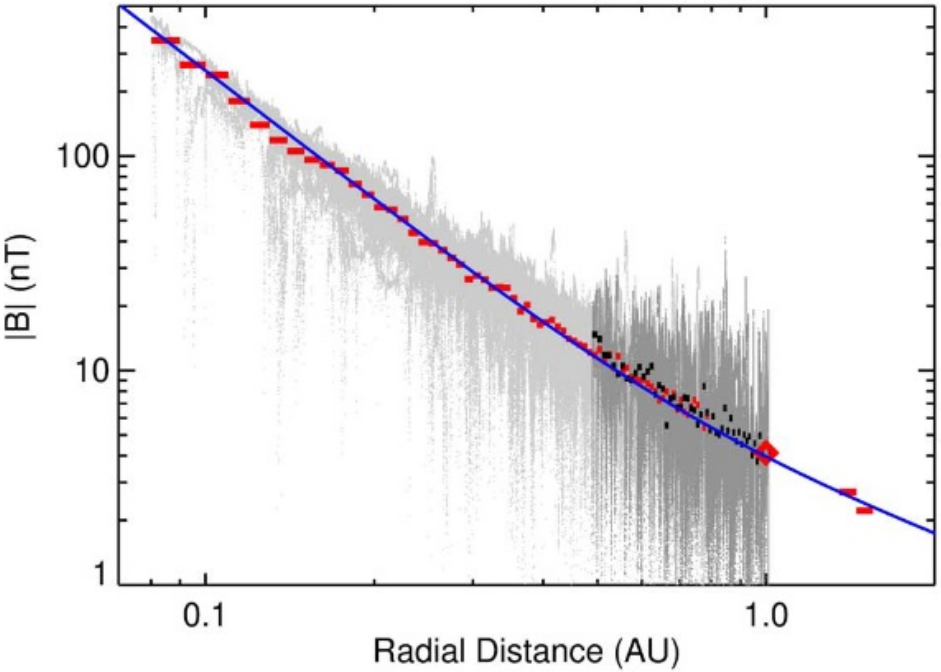


Figure 10.6: *Radial evolution of the interplanetary magnetic field strength (Parker spiral), $|\vec{\mathbf{B}}|$ measured by Parker Solar Probe from Safrankova et al 2023. The blue line is the analytical expression (10.4).*

10.8 Alfven radius/Alfven surface

While deriving the Parker magnetic field, magnetic field was assumed to be dragged by the plasma of the solar wind, i.e.

$$\underbrace{\frac{B^2}{2\mu_0}}_{Magnetic} < \underbrace{\frac{\rho v_{sw}^2}{2}}_{dynamicpressure}$$

so the solar wind speed must be larger than Alfven speed, $v > v_A = \frac{B}{\sqrt{\mu_0 \rho}}$ or the solar wind is **super-Alfvenic** above some distance $r > r_0$.

The Alfven surface divides the regions $v_A > v_{sw}$ for $r < r_0$ where the plasma follows the field co-rotating with the Sun and $v_A < v_{sw}$, where the magnetic field is following plasma forming Parker spiral (see Equation 10.4). This normally happens at 10-20$R_\odot$. NASA Parker Solar probe had passed the Alfvén critical surface in 2021.

11 Plasma turbulence and coronal heating

LECTURE OUTLINE

- Alfven waves
- Plasma turbulence
- Coronal heating and solar wind acceleration

11.1 Solar wind speed fluctuations

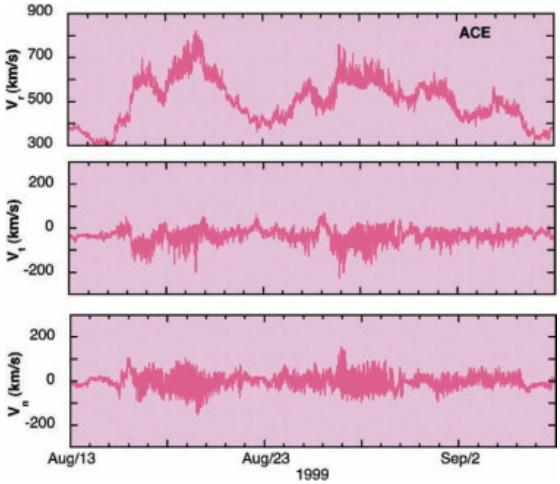


Figure 11.1: *Solar wind velocity data, radial outward direction from the Sun (r), the direction of the Earth's motion about the Sun (t), n direction completes a right-handed system. Gosling, Encyclopedia of the Solar System, 2007*

The solar wind is filled with waves and turbulence having various spatial and temporal scales. Figure 11.1 illustrates that fluctuations in solar wind velocity associated with waves and turbulence are observed throughout much of the solar wind, but fluctuation amplitudes tend to be greatest in high-speed streams.

Many of these fluctuations are Alfvénic in nature (coupled changes in flow velocity and magnetic field vectors) and the waves and turbulence usually are propagating away from the Sun through the solar wind; together with the fact that fluctuation ampli-

tudes generally decrease with distance from the Sun, this indicates that many of these fluctuations originate close to the Sun.

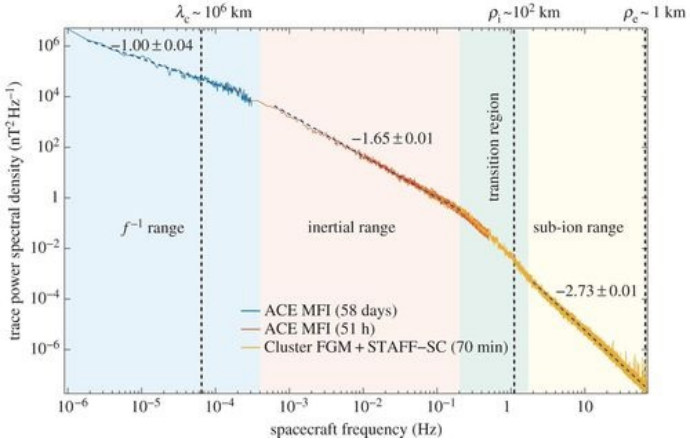


Figure 11.2: *Spectrum of turbulence measured in solar wind from Kiyani et al 2015.*

The high-frequency fluctuations in the representative 25-day interval are caused by waves and turbulence in the wind.

Solar wind fluctuations appear to be characterized by Alfvén waves Belcher and Davis, 1971.

Alfven waves are prorogating away from the Sun and dissipate their energy via turbulent cascade that leads to heating and wind acceleration.

11.2 Turbulence and energy cascade

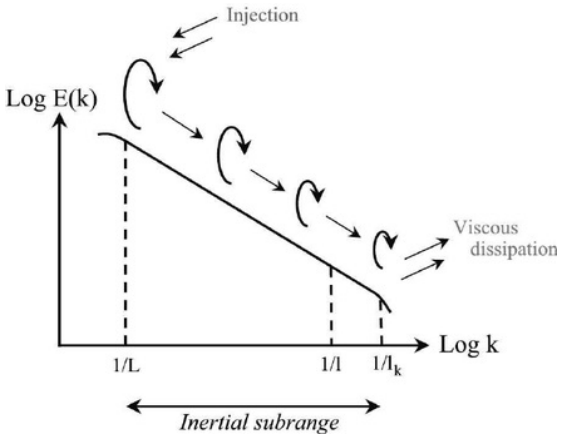


Figure 11.3: *Schematic illustration of production, energy cascade and dissipation in the energy spectrum of turbulence.*

The energy spectrum of turbulence, $E(k)$, is related to the mean turbulence kinetic energy per unit mass $\propto \rho\delta v^2/\rho$ as

$$\frac{1}{2}\overline{\delta v^2} = \int_0^\infty E(k)dk, \qquad (11.1)$$

where δv are the components of the fluctuating velocity, the overbar denotes an ensemble average, and k is the wavenumber. The energy spectrum, $E(k)$, thus represents the contribution to turbulence kinetic energy by wavenumbers from k to $k + dk$. The largest eddies have low wavenumber, and the small eddies have high wavenumbers.

11.3 Scaling arguments and Kolmogorov spectrum

Given the eddy interaction/turnover time is $\tau \simeq 1/(vk) = l/v$, the cascade energy transfer rate in isotropic turbulence

$$\epsilon = \frac{\text{energy}}{\text{time}} \simeq \frac{\delta v^2}{\tau} = \frac{\delta v^3}{k} \tag{11.2}$$

Let us assume no energy dissipation between injection and dissipation scales, then

$$\epsilon \simeq \frac{\delta v^3}{k} = \text{const} \quad \Rightarrow \quad \delta v \simeq \epsilon^{1/3} k^{-1/3} \tag{11.3}$$

and the energy spectrum of Kolmogorov turbulence

$$E(k) = \frac{\delta v^2}{k} \simeq \epsilon^{2/3} k^{-5/3} \tag{11.4}$$

which is the famous **Kolmogorov spectrum**. From Equation 11.3, the cascade or energy transfer time becomes $\tau \simeq 1/(\delta v k) \propto k^{-2/3}$. The spectrum is **universal**, independent of large-scale driving and small-scale dissipation.

11.4 Alfven waves

In magnetised plasma, and as observed in the solar wind, the large scale fluctuations are Alfvenic

$$\frac{\delta v}{v_A} \simeq \frac{\delta B}{B} \tag{11.5}$$

so propogate in plasma with speed v_A. In **Iroshnikov-Kraichnan** phenomenology, the interaction time is longer than in Kolmogorov phenomenology $\tau_K = (\delta v k)^{-1}$

$$\tau_{IK} \simeq \frac{1}{\delta v k}\frac{v_A}{\delta v} = \frac{v_A}{\delta v^2}k^{-1} \tag{11.6}$$

so assuming constant energy rate $\delta v^2/\tau_{IK} = \epsilon$, one finds $\delta v \propto \epsilon^{1/4}k^{-1/4}$ and Iroshnikov-Kraichnan spectrum becomes

$$E(k) = \frac{\delta v^2}{k} \propto \epsilon^{1/2}k^{-3/2} \tag{11.7}$$

which is flatter than Kolmogorov spectrum.

11.5 Solar wind spectrum

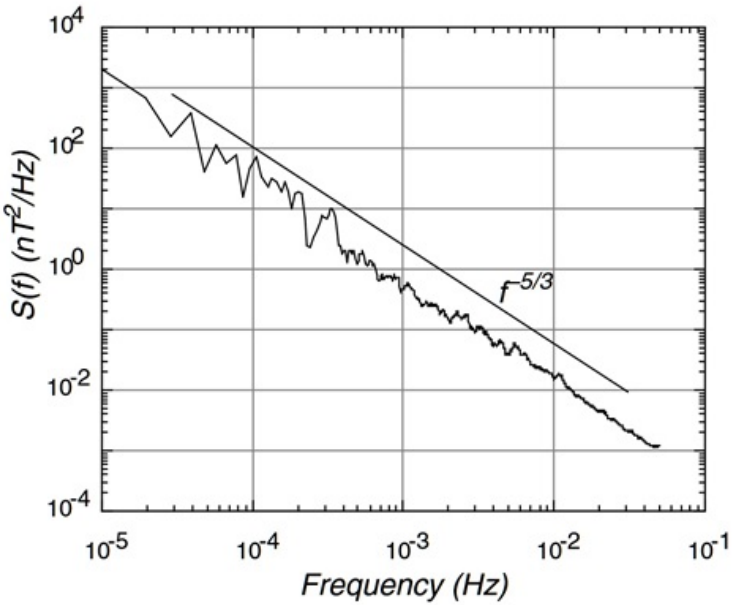


Figure 11.4: *A power spectrum of Voyager 2 data from 10 AU. A line with slope of −5/3 is shown for comparison from Goldstein, 2001.*

In-situ observations in the solar wind, show the spectrum of turbulence (Figure 11.4). As the solar wind moves with v_{sw}, so the spatial spectrum $E(k)$ is recorded by spacecraft as frequency spectrum and

$$kv_{sw} = 2\pi f \qquad (11.8)$$

In general, the direction of motion of solar wind is not constant and the orientation of the wavevectors with respect to solar wind velocity should be taken into account.

11.6 Goldreich-Sridhar spectrum

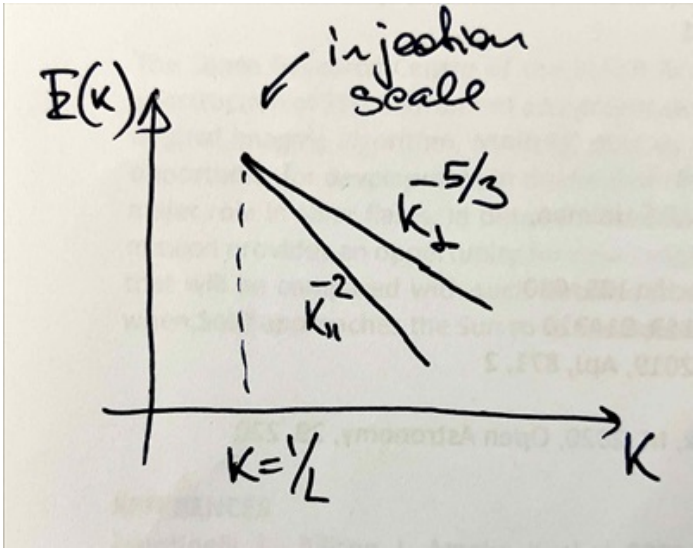


Figure 11.5: *Goldreich-Sridhar spectra*

Goldreich-Sridhar theory of strong Alfven-wave turbulence suggests that perpendicular to guiding magnetic field cascades with Kolmogorov timescale $(k_\perp \delta v)^{-1}$, but the spectrum along field lines with $(v_A k_\parallel)^{-1}$, so

$$E_{GS}(k_\perp) \propto k_\perp^{-5/3}, \quad E_{GS}(k_\parallel) \propto k_\parallel^{-2} \tag{11.9}$$

and there is **critical balance** between these two scales

$$(v_A k_\parallel)^{-1} \simeq (k_\perp \delta v)^{-1} \tag{11.10}$$

that suggest MHD cascade is anisotropic with scale-dependent anisotropy

$$k_\parallel \propto k_\perp^{-2/3} \tag{11.11}$$

Solar wind observations suggest anisotropic turbulence, but the details of the turbulence are under investigation.

11.7 Effects of Alfven turbulence

Alfven waves are weakly absorbed in plasma, so can propagate large distances. However, the Alfven wave interactions can lead to a turbulent cascade from large scales to small scales, where the energy is absorbed (ions and electrons are heated).

MHD turbulence is believed to be a critical ingredient to explain coronal/solar wind heating problem and acceleration of the solar wind.

MHD turbulence plays a key role in solar flares, coronal mass ejections, magnetic reconnection at the Sun and in a variety of astrophysical phenomena.

The details of development and dissipation of MHD turbulence are not fully understood and actively investigated in Astrophysics.